ORGANOMETALLICS

pubs.acs.org/Organometallics

Article

Tethering Carbohydrates to the Vinyliminium Ligand of Antiproliferative Organometallic Diiron Complexes

Silvia Schoch,[‖] Dalila Iacopini,[‖] Maria Dalla Pozza,[‖] Sebastiano Di Pietro, Ilaria Degano, Gilles Gasser,* Valeria Di Bussolo,* and Fabio Marchetti*

Cite This: *Organometallics* 2022, 41, 514−526

Read Online

ACCESS | Metrics & More | Article Recommendations | Supporting Information

ABSTRACT: Four propargyl *O*-glycosides derivatized with mannose, glucose, and fructose moieties were synthesized and then incorporated within a diiron structure as part of a vinyliminium ligand. Hence, six glycoconjugated diiron complexes, [**2**−**5**]CF_3SO_3 (see Scheme 1) and the nonglycosylated analogues [**6a**−**b**]CF_3SO_3, were obtained in high yields and unambiguously characterized by elemental analysis, mass spectrometry, and IR and multinuclear NMR spectroscopies. All compounds exhibited a significant stability in DMSO-d_6/D_2O solution, with 63−89% of the complexes unaltered after 72 h at 37 °C and also in the cell culture medium. The cytotoxicity of [**2**−**6**]CF_3SO_3, as well as that of previously reported **7** and **8**, was assessed on CT26 (mouse colon carcinoma), U87 (human glioblastoma), MCF-7 (human breast adenocarcinoma), and RPE-1 (human normal retina pigmented epithelium) cell lines. In general, the IC_{50} values correlate with the hydrophobicity of the compounds (measured as octanol−water partition coefficients) and do not show an appreciable level of selectivity against cancer cells with respect to the nontumor ones.

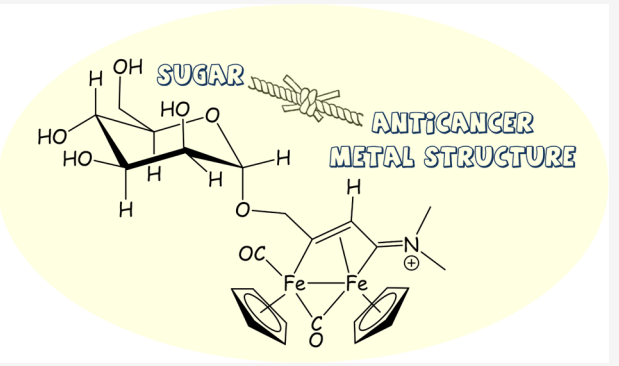

INTRODUCTION

A wide range of transition-metal complexes have been evaluated for their anticancer properties[1] with the aim of developing new effective drugs able to overcome the limitations associated with platinum compounds, which are massively administered in the clinic against several types of tumors.[2] Among the different categories of transition-metal complexes, iron complexes based on the ferrocene scaffold have aroused notable interest in recent years,[3] and especially, ferrocifens emerged, resulting from the conjugation of the ferrocene skeleton with the drug tamoxifen (Figure 1, structure **I**).[3,4] The antiproliferative activity of these compounds is ascribable to the redox chemistry of the ferrocenyl iron(II) center, which undergoes oxidation to Fe^{III} in the tumor cells, thus enhancing the formation of toxic metabolites leading to cell death.[5] Furthermore, "piano-stool" monoiron complexes, containing one cyclopentadienyl moiety and variable coligands (structure **II** in Figure 1), exert in some cases strong in vitro cytotoxicity against tumor cell lines.[6] Otherwise, the anticancer properties of di-organoiron complexes have been less explored,[7] despite the fact that a diiron carbonyl core constitutes the active unit of impressively efficient enzymes (i.e., hydrogenases),[8] in agreement with the general principle that suitable bimetallic systems enable reactivity patterns not accessible in homologous monometallic compounds.[9] The commercially available $[Fe_2Cp_2(CO)_4]$ (Cp = η^5-C_5H_5) is a convenient entry into diiron organometallic chemistry.[10] In particular, carbonyl ligands can be sequentially replaced by small molecular pieces, which are assembled, generating unusual bridging hydrocarbyl ligands stabilized by means of multisite coordination.[11] Thus, cationic μ-aminocarbyne complexes (Figure 1, structure **III**) are accessible by multigram-scale procedures[12] and represent the starting point to obtain vinyliminium derivatives (structure **IV**) via CO/alkyne substitution, featured by a notable structural variability.[13] Complexes belonging to the families **III**[14] and **IV**[15] possess a variable antiproliferative activity related to a multitargeted mechanism of action, with prevalent imbalance of cell redox homeostasis.

A general strategy to optimize the activity of anticancer metal complexes consists in the attachment of an organic fragment with documented biological activity to the metal scaffold.[16] Recently, we applied this approach to obtain diiron vinyliminium complexes **IV** derivatized with aspirin and

Received: September 14, 2021
Published: February 28, 2022

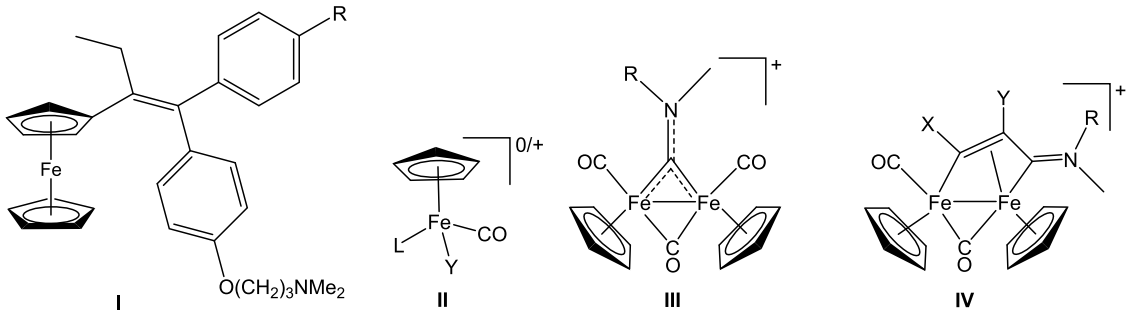

Figure 1. Structures of cyclopentadienyl iron complexes with anticancer activity: (**I**) ferrocifen (R = H, OH); (**II**) piano-stool monoiron complexes (L, Y = CO, phosphine, halide/pseudohalide); diiron complexes with a (**III**) bridging aminocarbyne or (**IV**) vinyliminium ligand (R = alkyl or aryl; R′ = alkyl, aryl, CO_2Me, 2-thiophenyl, pyridyl; R″ = H, CO_2Me, Ph, Me; triflate salts).

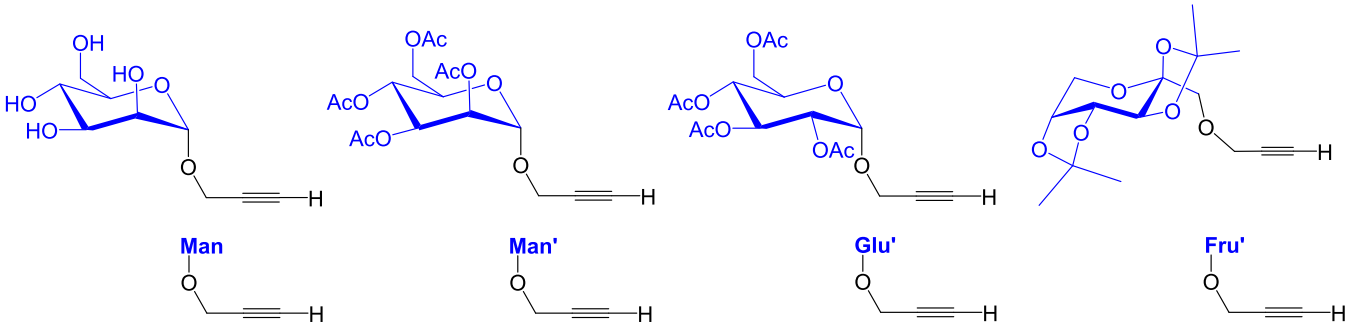

Figure 2. Propargyl *O*-glycosides employed in this work (HC≡CCH_2OMan and HC≡CCH_2OMan′ as mannose derivatives; HC≡CCH_2OGlu′ as glucose derivative; HC≡CCH_2OFru′ as fructose derivative).

chlorambucil, showing a clear influence of the bioactive moiety on the cytotoxicity profiles of the resulting complexes.[17]

The selective delivery of metal complexes to a specific kind of cells based on the metabolic features of the latter is a challenging goal, which may be useful for several purposes, including the therapy of pathological states such as cancer. In particular, tumor cells display a high avidity for carbohydrates, especially glucose, to sustain their high proliferation rate, which causes an increased glycolytic activity (Warburg effect).[18] As a consequence of this significantly increased request of glucose, as energy and bioprecursor sources, cancer cells commonly overexpress glucose transporters (GLUTs) on their cellular membrane surface.[19] In general, the attachment of carbohydrates to metal structures (either platinum complexes[20] or not[21]) represents a smart strategy, which potentially exploits GLUT-mediated cell uptake, and carbohydrate−metal complexes generally display enhanced biocompatibility, hydrophilicity (solubility), and pharmacokinetic parameters compared to the nonconjugated counterparts. Other carbohydrates in addition to D-glucose, such as D-mannose and D-fructose as well as OH-protected monosaccharides, can be direct substrates, or their bioprecursors, of GLUT transporters and thus can be considered as candidates for a GLUT-targeting approach.[18b,22] To date, only a few carbohydrate-containing iron complexes have been proposed as anticancer drug candidates.[23]

Here, we describe the straightforward synthesis of new diiron vinyliminium complexes derivatized with selected glucose, mannose, and fructose units, the evaluation of their behavior in aqueous media, and the assessment of their cytotoxicity toward a panel of cell lines.

RESULTS AND DISCUSSION

Synthesis and Characterization of Complexes. Propargyl *O*-glycosides (Figure 2) were prepared from the corresponding commercially available monosaccharides using optimized literature procedures (see the Supporting Information for details).[24,25]

Hence, diiron complexes with different carbohydrate-functionalized vinyliminium bridging ligands, [**2**−**5**]CF_3SO_3, were prepared from the easily available aminocarbyne precursors [**1a**−**b**]CF_3SO_3 (Scheme 1). First, one carbonyl ligand is replaced with the relatively labile acetonitrile molecule using the trimethylamine N-oxide strategy to give the adducts [**1′a**−**b**]CF_3SO_3 (Scheme 1). The subsequent reaction with the propargyl *O*-glycosides results in acetonitrile displacement by the alkyne function, immediately followed by regiospecific alkyne insertion into the iron−carbyne bond, affording [**2**−**5**]CF_3SO_3. By this method, complex [**2**]CF_3SO_3 obtained was impure; its successful preparation was achieved via intermediate acetonitrile/chloride substitution (formation of **1a-Cl**), followed by chloride abstraction with silver triflate in the presence of the alkyne HC≡CCH_2OMan. Complexes [**6a**−**b**]CF_3SO_3, containing a methyl group in the place of the monosaccharide moiety, were also prepared as reference compounds.

Novel compounds [**2**−**6**]CF_3SO_3 were isolated in 85−95% yields after work-up and fully characterized. Mass spectra confirmed the identity of the glycosylated compounds, clearly showing the peak related to the cation.

IR spectra of [**2**−**6**]CF_3SO_3 (Figures S9−S17) were recorded in dichloromethane solution except for [**2**]CF_3SO_3 (methanol): they share the typical pattern of diiron vinyliminium complexes[13,15,26] with two intense bands related to the terminal and bridging carbonyl ligands (in the ranges

https://doi.org/10.1021/acs.organomet.1c00519
Organometallics 2022, 41, 514−526

Scheme 1. Synthesis of Glycoconjugated Diiron Vinyliminium Complexes ($CF_3SO_3^-$ Salts) via Coupling of a Bridging Aminocarbyne Ligand with the Alkyne Function Belonging to Carbohydrate-Functionalized Propargyl *O*-Glycosides

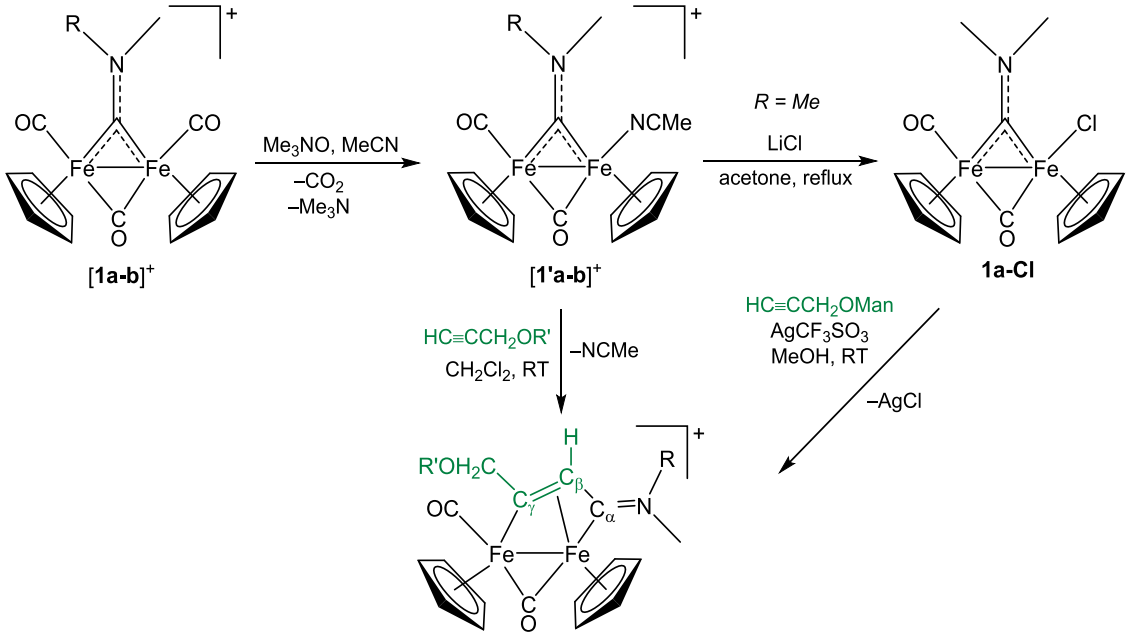

	R	*R'*
[**2**]+	Me	Man
[**3a**]+	Me	Man'
[**3b**]+	Xyl	Man'
[**4**]+	Me	Glu'
[**5a**]+	Me	Fru'
[**5b**]+	Xyl	Fru'
[**6a**]+	Me	Me
[**6b**]+	Xyl	Me

1989−2002 and 1808−1816 cm^{-1}, respectively) and a less intense absorption accounting for the iminium (C_α−N) bond. The latter is affected mainly by the nature of the iminium substituent R, and it falls at ca. 1680 and 1630 cm^{-1} for R = Me and R = Xyl, respectively. In addition, the spectra of [**3a**−**b**]CF_3SO_3 and [**4**]CF_3SO_3 show the band due to the acetyl groups within the carbohydrate fragment around 1750 cm^{-1}.

NMR spectra of [**2**−**5**]CF_3SO_3 (in acetone-d_6 or $CDCl_3$, Figures S19−S30) revealed the presence of two species in an almost equimolar ratio, and a plausible explanation is given in the following. The formation of the diiron vinyliminium core is not stereoselective, leading to a couple of enantiomers, which were recognized in many crystallographic structures (Figure 3).[13,15,26] In the present case, the two enantiomers combine with the enantiopure carbohydrate (Figure 2), giving rise to a couple of diastereomers.

Apart from the chirality issue mentioned above, the NMR spectra of [**2**−**6**]CF_3SO_3 suggested the highly regio- and stereoselective character of the alkyne insertion reaction. In fact, in the ^1H NMR spectra, the C_β−H hydrogen resonates within the interval of 4.5−5.3 ppm, whereas no signals were found at low fields typical for a bridging alkylidene ($C_\gamma H$, >9 ppm).[26,27] The Cp rings were seen as singlets in the range 5.06−5.74 ppm, which is indicative of a cis arrangement, upon comparison with a library of data available for homologous non glycosylated complexes.[13,15,17,26] Moreover, the unequal iminium substituents in [**3b**]CF_3SO_3 and [**5b**]CF_3SO_3 (R = Xyl) adopt the E geometry. Instead, [**6b**]CF_3SO_3 exists as a

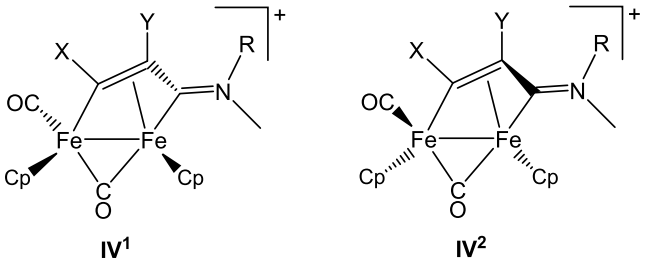

Figure 3. Diiron vinyliminium core is generally obtained as a couple of enantiomers due to the stereogenic iron centers.

mixture of E and Z isomers (additional Cp resonance at 4.83 ppm), with large prevalence of the former. The diastereotopic proton atoms belonging to the {C_γ-CH_2O} unit were detected in the 6.0−6.5 ppm range for [**2**−**5**]CF_3SO_3, mostly as a set of three/four signals, in accordance with the presence of two sugar-induced diastereomers. On the other hand, in [**6a**−**b**]CF_3SO_3, two doublets were clearly observed in the 5.5−6.0 ppm range, since the {C_γ-CH_2O} hydrogens are diastereotopically anisochronous even in the absence of the enantiopure carbohydrate moiety. In every case, the ^1H NMR window on the carbohydrate fragment reflects the fully *J*-coupled complexity typical of a pyranosic system: thus, in [**3**−**5**]CF_3SO_3, a series of signals occur in the 4.0−5.5 ppm region, being slightly shielded (3.5−4.5 ppm) in the mannose complex [**2**]CF_3SO_3 due to the absence of acetyl protection.

https://doi.org/10.1021/acs.organomet.1c00519
Organometallics 2022, 41, 514−526

From the ^{13}C NMR spectra of [**3**−**5**]CF_3SO_3, the anomeric diagnostic signal can be highlighted in the 95−100 ppm range; as for ^1H NMR spectra, most of the resonances related to the carbohydrate unit (60−80 ppm range) are doubled because of the pair of diastereomeric complexes. Salient features are represented by the resonances of C_α and C_γ, falling within the intervals of 225.1−233.4, and 199.3−206.9 ppm, respectively. These values account for the (amino)alkylidene nature of C_α and the alkylidene nature of C_γ, coherently with that reported for a vast series of non glycosylated vinyliminium complexes.[13,15]

Solubility, Stability in Aqueous Solutions, and Octanol−Water Partition Coefficients. Complexes [**2**]CF_3SO_3 and [**3a**]CF_3SO_3 exhibited the highest water solubility, which could be quantified in D_2O by ^1H NMR using dimethylsulfone (Me_2SO_2) as a standard (6.1 and 2.0 g·L^{-1}, respectively).[28,29] While [**2**]CF_3SO_3 is well soluble in methanol and acetone, it is limitedly soluble in dichloromethane, almost insoluble in chloroform, and insoluble in diethyl ether. Complex [**3a**]CF_3SO_3 is well soluble in chlorinated solvents and insoluble in diethyl ether, which facilitated the purification during work-up. The remaining compounds, [**3b**-**6**]CF_3SO_3, were slightly soluble in water, well soluble in dichloromethane and chloroform, and insoluble in diethyl ether.

According to ^1H NMR spectroscopy (Figures S35−S42), the compounds manifested a substantial stability in D_2O or D_2O/DMSO-d_6 solutions (^1H NMR), with up to 89% of the starting material recovered after 72 h at 37 °C (dimethylsulfone as standard, Table 1). The minor decomposition of the

Table 1. Fraction of the Residual Diiron Complex in the D_2O/DMSO-d_6 Mixture (2:1 v/v), Determined by ^1H NMR Spectroscopy (Me_2SO_2 as Internal Standard), and in RPMI, Determined by ESI-MS Analysis, after 72 h at 37 °C

compound	stability %	stability RPMI %
[**2**]CF_3SO_3	75[a]	0 (0[b])
[**3a**]CF_3SO_3	78[a]	43 (52[b])
[**3b**]CF_3SO_3	83	57 (77[b])
[**4**]CF_3SO_3	69	32 (54[b])
[**5a**]CF_3SO_3	89	78 (78[b])
[**5b**]CF_3SO_3	82	84 (84[b])
[**6a**]CF_3SO_3	78	94 (95[b])
[**6b**]CF_3SO_3	86	97 (97[b])

[a]D_2O solution. [b]Total amount of diiron complexes (starting complex + deacetylated derivatives).

complexes is featured by the precipitation of some solid, while newly formed organometallic species were not detected in solution. Semiquantitative electrospray-ionization mass spectrometry (ESI-MS) analyses suggested that most complexes are quite robust even in the cell culture medium. Briefly, each sample was dissolved in a small volume of DMSO and the solution was diluted with RPMI-1640 medium (final DMSO concentration < 5%). The mixtures were analyzed immediately after preparation and then stored at 37 °C for 72 h in the dark before new analyses. The interpretation of the spectra showed that complexes [**3a**−**b**]CF_3SO_3 and [**4**]CF_3SO_3 gradually released one/two protecting groups. In the spectra acquired after 72 h for [**5a**−**b**]CF_3SO_3, bearing the isopropylidene-protected fructose, and [**6a**−**b**]CF_3SO_3, lacking the carbohydrate function, the unaltered complex was the largely prevalent species detected. Interestingly, the hydrophilic and inactive complex [**2**]CF_3SO_3 (vide infra) exhibited a distinctive behavior, in that almost immediate degradation was recognized, presumably triggered by some medium component; in this case, the only diiron derivative, which could be detected in solution, albeit in a low concentration, is [**9a**]$^+$ (vide infra), resulting from the loss of the carbohydrate moiety. The stability of all complexes, expressed as the percentage of the compound retrieved after 72 h, is detailed in Table 1. According to these outcomes, it appears that the introduction of a nonprotected carbohydrate moiety within the vinyliminium moiety is totally detrimental to the stability of the diiron core; on the other hand, the choice of protected carbohydrates overcomes the stability issues and determines a progressive cleavage of the organometallic scaffold.

Octanol−water partition coefficients ($\mathrm{Log}\,P_{ow}$) of the complexes were measured by means of a UV−vis method (see Experimental Studies for details), and the obtained values are reported in Table 2. In general, the diiron complexes display a significant level of hydrophilicity, with [**2**]CF_3SO_3 being the most hydrophilic one ($\mathrm{Log}\,P_{ow}$ = −0.90). The iminium substituents strongly contribute, and for instance, $\mathrm{Log}\,P_{ow}$ for the homologous complexes [**5a**]CF_3SO_3 and [**5b**]CF_3SO_3 are −0.53 (R = Me) and +0.43 (R = Xyl), respectively. The introduction of the acetylated mannosyl moiety (R′ = Man′, complexes **3a**−**b**) produces almost the same effect, in terms of hydrophilicity, as the methyl group (R′ = Me, complexes **6a**−**b**).

Cytotoxicity Studies. The cytotoxicity of the novel diiron complexes [**2**−**6**]CF_3SO_3 was evaluated using increasing concentrations of the complexes against the cancer cell lines CT26, U87, and MCF-7 and the nontumoral cell line RPE-1. The concentration of the tested compounds inducing 50% reduction in the cell number compared to control cultures (IC_{50}) was determined using the resazurin assay. The previously reported diiron complexes [**7**]CF_3SO_3 and [**8**]CF_3SO_3[15a] (Figure 4) and cisplatin were used as references.

The results are compiled in Table 2, while dose−response cell viability curves are supplied as the Supporting Information (Figures S51−S54).

In general, data show a clear correlation between the cytotoxicity and the hydrophobicity of the glycoconjugated compounds and the absence of an appreciable selectivity. Instead, the degree of relative stability of the complexes (Table 1) does not appear to play a prominent role. Thus, [**2**]CF_3SO_3, [**3a**]CF_3SO_3, [**5a**]CF_3SO_3, and [**6a**]CF_3SO_3 are not cytotoxic in the concentration range of 0.01−100 μM against all of the tested cell lines, probably due to their substantial hydrophilic character (negative $\mathrm{Log}\,P_{ow}$ values), disfavoring cell penetration. The moderate cytotoxicity of [**4**]CF_3SO_3 ($\mathrm{Log}\,P_{ow}$ = −0.83) against the CT26 cell line emerges as an exception. The behavior of the mannosyl-peracetylated complex [**3b**]CF_3SO_3 may be compared with that of the analogous [**6b**]CF_3SO_3, lacking the carbohydrate moiety and featuring a close $\mathrm{Log}\,P_{ow}$ value. Thus, the two complexes display a comparable activity against the CT26 and U87 cell lines; otherwise, [**6b**]CF_3SO_3 is much more active against MCF-7 cells but less selective. On the other hand, nonglycosylated complexes [**7**]CF_3SO_3 ($\mathrm{Log}\,P_{ow}$ = 0.4) and [**8**]CF_3SO_3 ($\mathrm{Log}\,P_{ow}$ = 0.0) appear more effective than [**3b**]CF_3SO_3 ($\mathrm{Log}\,P_{ow}$ = −0.12), [**5b**]CF_3SO_3 ($\mathrm{Log}\,P_{ow}$ = 0.43), and [**6b**]CF_3SO_3 ($\mathrm{Log}\,P_{ow}$ = −0.19), suggesting that an appropriate choice of simple substituents on the vinyliminium chain

https://doi.org/10.1021/acs.organomet.1c00519
Organometallics 2022, 41, 514−526

Table 2. IC_{50} Values (Reported in μM) Obtained after 48 h of Continuous Incubation of Diiron Complexes and Cisplatin with U87, CT26, MCF-7, and RPE1 Cells[a]

compound	CT26	U87	MCF-7	RPE1	Log P_{ow}
[**2**]CF_3SO_3	>100	>100	>100	>100	−0.90 ± 0.06
[**3a**]CF_3SO_3	>100	>100	>100	>100	−0.71 ± 0.01
[**3b**]CF_3SO_3	20 ± 4	52 ± 15	>100	43 ± 9	−0.12 ± 0.01
[**4**]CF_3SO_3	48 ± 5	>100	>100	>100	−0.83 ± 0.01
[**5a**]CF_3SO_3	>100	>100	>100	>100	−0.53 ± 0.01
[**5b**]CF_3SO_3	6 ± 1	22 ± 3	23 ± 8	26 ± 17	0.43 ± 0.01
[**6a**]CF_3SO_3	>100	>100	>100	>100	−0.70 ± 0.01
[**6b**]CF_3SO_3	18 ± 8	81 ± 16	29 ± 13	24 ± 4	−0.19 ± 0.01
[**7**]CF_3SO_3	7 ± 1	6 ± 1	7 ± 1	8 ± 2	0.4[15a]
[**8**]CF_3SO_3	8 ± 1	17 ± 1	28 ± 1	28 ± 2	0.0[15a]
Cisplatin	0.8 ± 0.1	5.9 ± 1.4	19 ± 3	28 ± 4	

[a]On the right column, Log P_{ow} values are reported.

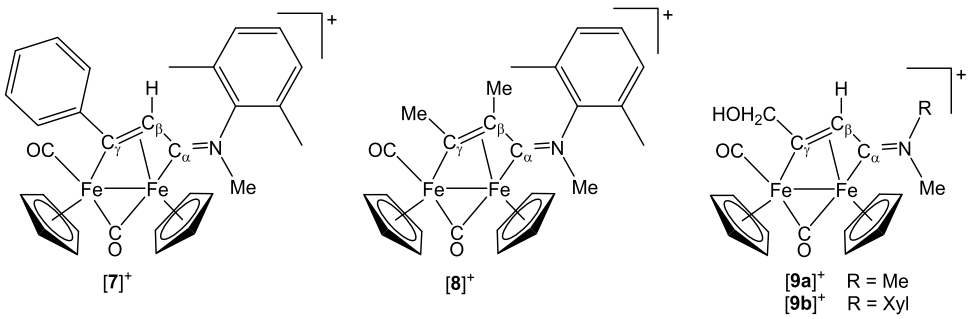

Figure 4. Previously reported diiron vinyliminium complexes analyzed or cited in this work (triflate salts).

might be more incisive than the incorporation of a carbohydrate moiety. In particular, the cytotoxicity of [**7**]-CF_3SO_3 exceeds that of cisplatin against the MCF-7 cell line, while comparable IC_{50} values have been recognized for these two compounds on the U87 cell line.

To evaluate if the absence of glucose in the medium could increase or somehow affect the cytotoxicity of the tested compounds, we investigated the difference in terms of IC_{50} between the normal conditions and the cells cultivated in no-glucose medium. In principle, in the latter condition, cells would experience a major demand for glucose (and carbohydrates in general) and may become more prone to internalize the functionalized diiron complexes, resulting in an increased cytotoxicity.[30] For this study, we selected the moderately active complexes [**3b**]CF_3SO_3 and [**5b**]CF_3SO_3, containing two different carbohydrate moieties, and [**6b**]-CF_3SO_3, which is not decorated with any sugar moiety. The collected observations pointed out no different values of IC_{50} comparing the glucose and no-glucose conditions, indicating that the activity of the compounds is not influenced by the absence of glucose (Table 3 and Figure S55). In other words, cell glucose transporters do not seem to be involved in the uptake of the diiron complexes.

The wound healing assay (also known as the scratch assay) is an economical and simple method to evaluate cell migration *in vitro*, mimicking the migration of cells *in vivo*.[31] We performed this assay on selected complexes to investigate their cell migration inhibitory potential. First, for each complex, the IC_{20} value (i.e., the concentration of the drug inhibiting 20% of the cell viability) was graphically determined from the respective plot of cell viability (Figures S51−S54). Then, CT26 colon carcinoma cells were treated with [**3b**]CF_3SO_3, [**5b**]CF_3SO_3, and [**6b**]CF_3SO_3 at the respective IC_{20} concentrations. The IC_{20} dose was used for each complex for the evaluation process, to affect the cells but avoiding any other kind of high concentration-dependent effect. After carefully scratching the cellular monolayer, the scratch was monitored to check the differences in the healing between cells treated with diiron complexes and nontreated cells. This qualitative comparison did not reveal a meaningful difference in terms of migration (Figure 5); in fact, the scratch was healed approximately to the same extent over 30 h in the distinct cases. We can conclude that the investigated diiron complexes are not capable of inhibiting the migration of the cells in the conditions used for the assay.

Table 3. IC_{50} Values (Reported in μM) Obtained after 48 h of Continuous Incubation of Diiron Complexes and Cisplatin with CT26 Cells, Cultivated with and without Glucose, Respectively

compound	with glucose	without glucose
[**3b**]CF_3SO_3	18 ± 3	15 ± 3
[**5b**]CF_3SO_3	10 ± 4	6.8 ± 0.7
[**6b**]CF_3SO_3	21 ± 2	10 ± 3
cisplatin	1.3 ± 0.2	0.7 ± 0.3

Overall, our findings suggest that diiron vinyliminium complexes [**2**−**8**]CF_3SO_3 exert their cytotoxicity inside the cells, in agreement with the absence of activity detected for the most hydrophilic complexes. The presence of a carbohydrate unit does not seem beneficial to the uptake, and a passive diffusion pathway could be hypothesized for the less hydrophilic complexes, but more studies are required to validate this hypothesis. In agreement with the previous reports, it is presumable that the cytotoxicity is triggered mainly by the intracellular disassembly of the diiron

https://doi.org/10.1021/acs.organomet.1c00519
Organometallics 2022, 41, 514−526

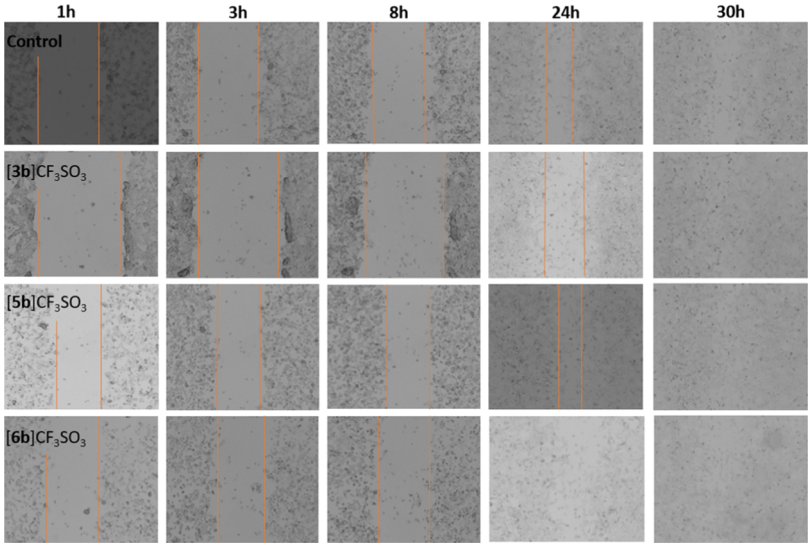

Figure 5. Migration of CT26 cells after 1, 3, 8, 24, and 30 h, following treatment with IC_{20} concentrations of [**3b**]CF_3SO_3, [**5b**]CF_3SO_3, and [**6b**]CF_3SO_3, respectively, or not (control). Orange lines indicate the edges of the scratches. In the experiment, we used less than 1% of DMSO containing Dulbecco's modified Eagle medium (DMEM) medium. The images are representative from one successive experiment out of three successive individual experiments.

scaffold,[7,15,17] with the release of iron(I) ions contributing to the imbalance of the cell redox homeostasis.[14,32] In this regard, the complete inactivity of the highly unstable complex [**2**]CF_3SO_3 agrees in that, to supply an antiproliferative effect, the degradation must be operative inside the cell. The slightly lower performance exhibited by the relatively lipophilic carbohydrate complexes, compared to the nonfunctionalized ones [**7**−**8**]CF_3SO_3, might be related to some interference of the carbohydrate function with degradation routes, which appear essential to the drug activity (see above). In addition, the possible cleavage of the glycosidic bond inside the cell would lead to vinyliminium derivatives containing a {CH_2OH} function; in this regard, it has to be noted that complexes [**9a**−**b**]$^+$ (Figure 4), which would be generated by this process from [**3**]$^+$ and [**5**]$^+$, respectively, were previously found to be considerably less active and less selective than the related complexes with other C_γ substituents.[15a]

CONCLUSIONS

Conjugation with carbohydrates is a well-established strategy to improve anticancer activity of transition-metal complexes, essentially aimed at increasing the drug uptake by cancer cells. Here, we report the incorporation of alkynes functionalized with different monosaccharide moieties within a di-organoiron scaffold, which was previously demonstrated to exert promising in vitro cytotoxicity. Antiproliferative activities of the new complexes on a panel of cancer cell lines correlate with their lipophilicity, ranging from moderate to inactive and showing an absence of appreciable selectivity with respect to a nontumoral cell line. On the other hand, analogous diiron complexes with different substituents on the bridging vinyliminium ligand, analyzed as references, performed better in the same conditions, thus confirming the potential of the present category of organometallics in the medicinal field. The absence of a clear favorable effect of the carbohydrate moiety may be a consequence of adverse steric factors, disfavoring the interaction of the encumbered diiron scaffold with GLUT transporters and thus hampering the transport of the complexes through the cell membrane.[18b]

However, the versatility of the diiron structure and the very general character of the alkyne insertion reaction affording vinyliminium ligands, demonstrated also in the present work, may constitute a notable potential for the design and future development of optimal iron drug candidates.

EXPERIMENTAL STUDIES

Synthesis and Characterization of Compounds. *General Details.* All operations were conducted in air, unless otherwise specified. Once isolated, all of the products were stored in air, except the hygroscopic complex [**2**]CF_3SO_3, which was stored under N_2. Organic reactants were purchased from TCI Europe or Merck and were of the highest purity available, while solvents were purchased from Merck (petroleum ether, bp = 40−60 °C). The synthesis and characterization of propargyl *O*-glycosides are provided as the Supporting Information. Complexes [$Fe_2Cp_2(CO)_2(\mu$-CO){μ-CNMe(R)}]CF_3SO_3 (R = Me, [**1a**]CF_3SO_3; R = Xyl = 2,6-$C_6H_3Me_2$, [**1b**]CF_3SO_3),[12] [$Fe_2Cp_2(CO)(\mu$-CO){μ-η^1:η^3-C_γ(Ph)-$C_\beta HC_\alpha N$(Me)(Xyl)}]CF_3SO_3 (**7**),[15a] and [$Fe_2Cp_2(CO)(\mu$-CO){μ-η^1:η^3-C_γ(Me)C_β(Me)C_αN(Me)(Xyl)}]CF_3SO_3 (**8**)[15a] were prepared according to the respective literature procedures. Separations were carried out on columns of silica (Merck), deactivated alumina (Merck, 4% w/w water), or celite (Fluka, 512 Medium). Infrared spectra of solutions were recorded on a PerkinElmer Spectrum 100 FT-IR spectrometer with a CaF_2 liquid transmission cell (2300−1500 cm^{-1} range) or on solid samples at 298 K on a PerkinElmer FT-IR spectrometer, equipped with a UATR sampling accessory. UV−vis spectra were recorded on an Ultraspec 2100 Pro spectrophotometer. IR and UV−vis spectra were processed with Spectragryph software.[33] NMR spectra were recorded at 298 K on a Bruker Avance II DRX400 instrument equipped with a BBFO broadband probe. Chemical shifts (expressed in parts per million) are referenced to the residual solvent peaks (^{1}H, ^{13}C).[34] NMR spectra were assigned with the assistance of ^{1}H−^{13}C (*gs*-HSQC and *gs*-HMBC) correlation experiments.[35] NMR signals due to secondary isomeric forms (where it has been possible to detect them) are italicized. Elemental analyses were performed on a Vario MICRO cube instrument (Elementar). Electrospray-ionisation quadrupole time-of-flight (ESI-Q-ToF) flow injection analyses (FIA) were carried out using a 1200 Infinity HPLC (Agilent Technologies), coupled to a Jet Stream ESI interface (Agilent) with a quadrupole-time of flight tandem mass spectrometer 6530 Infinity Q-TOF (Agilent Technologies). High-performance liquid chromatography-

https://doi.org/10.1021/acs.organomet.1c00519
Organometallics 2022, 41, 514−526

mass spectrometry (HPLC-MS) grade acetonitrile was used as the mobile phase (Carlo Erba, Italy). The flow rate was 0.2 mL min^{-1} (total run time 3 min). The ESI operating conditions were: drying gas (N_2, purity > 98%): 350 °C and 10 L·min^{-1}; capillary voltage: 4.5 kV; nozzle voltage: 1 kV; nebulizer gas: 35 psig; sheath gas (N_2, purity > 98%): 375 °C and 11 L min^{-1}. The fragmentor was kept at 50 V, the skimmer at 65 V, and the OCT 1 RF at 750 V. High-resolution ESI-MS spectra were achieved in positive mode in the range 100−1700 m/z; the mass axis was calibrated daily using the Agilent tuning mix HP0321 (Agilent Technologies) prepared in acetonitrile and water.

Synthesis and Characterization of $[Fe_2Cp_2(Cl)(CO)(\mu\text{-}CO)\{\mu\text{-}CNMe_2\}]$, 1a-Cl (Figure 6). The title compound was prepared using a modified literature procedure.[36] A solution of $[\mathbf{1a}]CF_3SO_3$ (1.02 g, 1.92 mmol) in acetonitrile (15 mL) was treated with Me_3NO (188 mg, 2.50 mmol), and the resulting solution was stirred for 2 h, enabling the release of produced gas (CO_2, Me_3N). The complete conversion of $[\mathbf{1a}]CF_3SO_3$ into the acetonitrile adduct $[\mathbf{1'a}]CF_3SO_3$[36] was checked by IR spectroscopy. The volatiles were eliminated under reduced pressure, affording a dark-brown residue, which was dissolved into acetone (30 mL). Lithium chloride (132 mg, 3.11 mmol) was added, and the resulting mixture was heated at reflux for 2 h. The complete conversion of the acetonitrile adduct into **1a-Cl** was checked by IR spectroscopy in CH_2Cl_2 solution. After removal of the solvent under reduced pressure, the residue was dissolved in dichloromethane and filtered on a celite pad under N_2 atmosphere. The solvent removal under vacuum led to recover the title compound as a light-brown solid. Yield 559 mg (75%). Anal. calcd for $C_{15}H_{16}ClFe_2NO_2$: C, 46.26; H, 4.14; N, 3.60. Found: C, 46.35; H, 4.16; N, 3.48. IR (CH_2Cl_2): $\tilde{\nu}/cm^{-1}$ = 1978vs (CO), 1800s (μ-CO), 1575m (μ-CN). ^1H NMR ($CDCl_3$): δ/ppm = 4.76, 4.68 (s, 10 H, Cp); 4.73, 4.28 (s, 6H, NMe_2) (Figure 6).

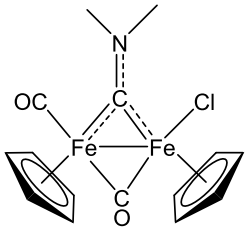

Figure 6. Structure of **1a-Cl**.

Synthesis and Characterization of Diiron Vinyliminium Complexes. *$[Fe_2Cp_2(CO)(\mu\text{-}CO)\{\mu\text{-}\eta^1{:}\eta^3\text{-}C_\gamma(CH_2O\text{-}\alpha\text{-}Mannopyranosyl)C_\beta HC_\alpha NMe_2\}]CF_3SO_3$, $[\mathbf{2}]CF_3SO_3$ (Figure 7).* A mixture of **1a-Cl** (128 mg, 0.33 mmol) and $HC{\equiv}CCH_2OMan$ (72 mg, 0.33 mmol), in methanol (20 mL), was treated with $AgCF_3SO_3$ (86 mg, 0.33 mmol). The resulting mixture was stirred at room temperature for 70 min and then filtered on a celite pad to remove AgCl. The filtered solution was dried under reduced pressure. The obtained black residue was repeatedly washed with $CHCl_3$ and then evaporation of the solvent under reduced pressure afforded $[\mathbf{2}]$-CF_3SO_3 as a hygroscopic black solid. This solid was dissolved in MeOH (2 mL) under N_2 atmosphere and quickly precipitated by adding petroleum ether (25 mL). A black powder was isolated upon evaporation of the solvent under vacuum and then stored under N_2. Yield 212 mg (89%). Anal. calcd for $C_{25}H_{30}F_3Fe_2NO_{11}S$: C, 41.63; H, 4.19; N, 1.94. Found: C, 41.24; H, 4.29; N, 1.82. HR-ESI-MS: $[M]^+$ m/z = 572.0663 (theoretical for $[C_{24}H_{30}Fe_2NO_8]^+$: m/z = 572.0670; error: −1.2 ppm). IR (CH_3OH): $\tilde{\nu}/cm^{-1}$ = 1989vs (CO), 1813s (μ-CO), 1688m ($C_\alpha N$). ^1H NMR (acetone-d_6): δ/ppm = 6.40−5.88 (m, 2 H, $C_\gamma CH_2$); 5.55, 5.22 (s, 10 H, Cp); 5.52 (m, 1 H, H^1); 5.29, 4.30−3.80 (m, 6 H, $H^2 + H^3 + H^4 + H^5 + H^6$); 5.25 (s, 1 H, $C_\beta H$); 3.97, 3.37 (s, 6 H, NMe_2); 3.85−3.58 (s, 4 H, OH). Diastereomeric ratio = 1. $^{13}C\{^1H\}$ NMR (acetone-d_6): δ/ppm = 256.1 (μ-CO); 225.5 (C_α); 210.4 (CO); 201.3 (C_γ); 121.0 (q, $^1J_{C-F}$ = 321 Hz, CF_3); 101.0, 100.0 (C^1); 89.8, 87.5 (Cp); 88.5, 86.6, 74.1, 73.9, 71.7, 71.5, 71.0, 70.7 ($C^2 + C^3 + C^4 + C^5$); 80.3, 79.7 ($C_\gamma CH_2$); 61.7, 61.5 (C^6); 50.7, 44.4 (NMe_2); 47.3 (C_β) (Figure 7).

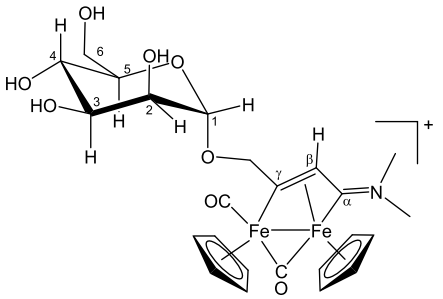

Figure 7. Structure of $[\mathbf{2}]^+$.

General Procedure for the Synthesis of $[\mathbf{3-5}]CF_3SO_3$. A solution of $[\mathbf{1a-b}]CF_3SO_3$ in MeCN (ca. 10 mL) was treated with Me_3NO (ca. 1.2 equiv). The resulting mixture was stirred for 50 min and progressive color darkening was observed. The complete conversion of the starting material into the corresponding acetonitrile adduct $[\mathbf{1'a-b}]CF_3SO_3$[36] was checked by IR spectroscopy. The volatiles were removed under vacuum to afford a dark-brown residue, which was dissolved in dichloromethane and treated with the selected alkyne. This solution was stirred at room temperature for 4 days, and then it was filtered through celite. The volatiles were evaporated from the filtered solution under reduced pressure; thus, the residue was repeatedly washed with diethyl ether and finally dried under vacuum. The synthesis of $[\mathbf{2}]CF_3SO_3$ using this procedure (from $[\mathbf{1a}]CF_3SO_3$) afforded the unclean product in ca. 72% yield.

$[Fe_2Cp_2(CO)(\mu\text{-}CO)\{\mu\text{-}\eta^1{:}\eta^3\text{-}C_\gamma(CH_2O\text{-}2,3,4,6\text{-}Tetra\text{-}O\text{-}acetyl\text{-}\alpha\text{-}mannopyranosyl)C_\beta HC_\alpha NMe_2\}]CF_3SO_3$, $[\mathbf{3a}]CF_3SO_3$ (Figure 8). From $[\mathbf{1'a}]CF_3SO_3$, freshly prepared from $[\mathbf{1a}]CF_3SO_3$ (91 mg, 0.17 mmol) and $HC{\equiv}CCH_2OMan'$ (91 mg, 0.24 mmol). Brown solid, yield 133 mg (87%). Anal. calcd for $C_{33}H_{38}F_3Fe_2NO_{15}S$: C, 44.56; H, 4.31; N, 1.57. Found: C, 44.38; H, 4.39; N, 1.70. HR-ESI-MS: $[M]^+$ m/z = 740.1094 (theoretical for $[C_{32}H_{38}Fe_2NO_{12}]^+$: m/z = 740.1093; error: 0.1 ppm). IR (CH_2Cl_2): $\tilde{\nu}/cm^{-1}$ = 1992s (CO), 1811m (μ-CO), 1750vs (C═O), 1680w ($C_\alpha N$). ^1H NMR (acetone-d_6): δ/ppm = 6.50−6.00 (m, 2 H, $C_\gamma CH_2$); 5.58, 5.58, 5.27, 5.26 (s, 10 H, Cp); 5.55−5.38, 5.19, 4.41 (m, 5 H, $H^1 + H^2 + H^3 - H^4 + H^5$); 5.24 (s, 1 H, $C_\beta H$); 4.30, 4.28 (m, 2 H, H^6); 3.99, 3.38, 3.38 (s, 6 H, NMe_2); 2.20−1.95 (s, 12 H, 4× O═CMe−). Diastereomeric ratio = 1. $^{13}C\{^1H\}$ NMR (acetone-d_6): δ/ppm = 255.3, 255.2 (μ-CO); 225.3 (C_α); 210.3, 210.2 (CO); 199.7, 199.3 (C_γ); 170.1, 169.8, 169.4 (4× O═CMe); 98.2, 97.3 (C^1); 89.8, 87.5, 87.5 (Cp); 80.1 ($C_\gamma CH_2$); 69.4, 69.3 ($C^3 + C^4 + C^5$); 65.9 (C^2); 62.6, 62.4 (C^6); 50.7, 44.4 (NMe_2); 47.6 (C_β); 19.9 (4× O═C*Me*) (Figure 8).

$[Fe_2Cp_2(CO)(\mu\text{-}CO)\{\mu\text{-}\eta^1{:}\eta^3\text{-}C_\gamma(CH_2O\text{-}2,3,4,6\text{-}Tetra\text{-}O\text{-}acetyl\text{-}\alpha\text{-}mannopyranosyl)C_\beta HC_\alpha N(Me)(Xyl)\}]CF_3SO_3$, $[\mathbf{3b}]CF_3SO_3$ (Figure 9). From $[\mathbf{1'b}]CF_3SO_3$, freshly prepared from $[\mathbf{1b}]CF_3SO_3$ (106 mg, 0.17 mmol) and $HC{\equiv}CCH_2OMan'$ (120 mg, 0.31 mmol). Brown solid, yield 152 mg (91%). Anal. calcd for $C_{40}H_{44}F_3Fe_2NO_{15}S$: C, 49.05; H, 4.53; N, 1.43. Found: C, 48.80; H, 4.67; N, 1.53. HR-ESI-

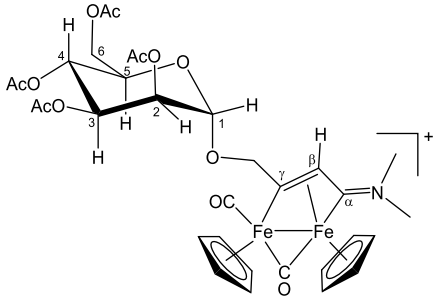

Figure 8. Structure of $[\mathbf{3a}]^+$.

https://doi.org/10.1021/acs.organomet.1c00519
Organometallics 2022, 41, 514−526

MS: $[M]^+$ m/z = 830.1561 (theoretical for $[C_{39}H_{44}Fe_2NO_{12}]^+$: m/z = 830.1562; error: −0.1 ppm). IR (CH_2Cl_2): $\tilde{\nu}$/cm^{-1} = 2002s (CO), 1816s (μ-CO), 1751vs (C═O), 1633m (C_αN). ^{1}H NMR (acetone-d_6): δ/ppm = 7.30−7.20, 7.08 (m, 3 H, C_6H_3); 6.38, 6.29, 6.15, 5.97 (d, $^2J_{HH}$ = 15.0 Hz, 2 H, $C_\gamma CH_2$); 5.74, 5.73, 5.48, 5.48 (s, 10 H, Cp); 5.69 (m, 1 H, H^1); 5.44−5.30 (m, 4 H, H^2 + H^3 + H^4 + H^5); 4.38 (s, 3 H, NMe); 4.27−4.10 (m, 2 H, H^6); 4.15 (s, 1 H, C_βH); 2.39, 2.36, 1.87, 1.86 (s, 6 H, $C_6H_3Me_2$); 2.16, 2.15, 2.10, 2.09, 2.03, 2.03, 2.02, 2.01 (s, 12 H, 4× O═CMe). Diastereomeric ratio = 1.2. ^{13}C{^{1}H} NMR (acetone-d_6): δ/ppm = 253.2, 253.0 (μ-CO); 232.7, 232.6 (C_α); 210.2, 210.1 (CO); 203.9, 203.5 (C_γ); 170.0, 169.9, 169.8, 169.8, 169.8, 169.6, 169.2 (4× O═*C*Me); 145.2, 145.2, 131.9, 131.3, 131.3 (*ipso*-C_6H_3); 129.6, 129.5, 129.4, 129.3, 129.2 (C_6H_3); 98.1, 97.1 (C^1); 90.6, 87.9, 87.8 (Cp); 80.5, 79.9 ($C_\gamma CH_2$); 69.5, 69.4, 69.3, 69.3, 69.2, 69.1 (C^3 + C^4 + C^5); 65.7, 65.6 (C^2); 62.3, 62.1 (C^6); 54.1 (C_β); 45.8, 45.8 (NMe); 19.9−19.7 (4× O═C*Me*); 17.1, 17.1, 16.6 ($C_6H_3Me_2$) (Figure 9).

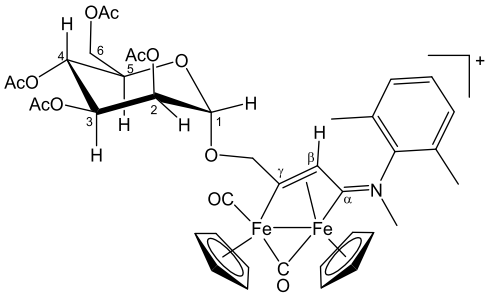

Figure 9. Structure of $[\mathbf{3b}]^+$.

*[$Fe_2Cp_2(CO)(\mu$-CO)$\{\mu$-η^1:η^3-C_γ(CH_2O-2,3,4,6-Tetra-O-acetyl-α-glucopyranosyl)$C_\beta HC_\alpha NMe_2$}] CF_3SO_3, [**4**]CF_3SO_3 (Figure 10).* From [**1′a**]CF_3SO_3, freshly prepared from [**1a**]CF_3SO_3 (69 mg, 0.13 mmol) and HC≡CCH_2OGlu′ (74 mg, 0.19 mmol). Dark-brown solid, yield 99 mg (85%). Anal. calcd for $C_{33}H_{38}F_3Fe_2NO_{15}S$: C, 44.56; H, 4.31; N, 1.57. Found: C, 44.68; H, 4.22; N, 1.65. IR (CH_2Cl_2): $\tilde{\nu}$/cm^{-1} = 1993m (CO), 1811m (μ-CO), 1753vs (C═O), 1682w (C_αN). HR-ESI-MS: $[M]^+$ m/z = 740.1093 (theoretical for $[C_{32}H_{38}Fe_2NO_{12}]^+$: m/z = 740.1093; error: 0.0 ppm). ^{1}H NMR (acetone-d_6): δ/ppm = 6.44−5.95 (m, 2 H, $C_\gamma CH_2$); 5.66−5.59, 5.24−5.16 (m, 3 H, H^1 + H^3 + H^4); 5.59, 5.56, 5.30, 5.28 (s, 10 H, Cp); 5.20 (s, 1 H, C_βH); 5.12 (dt, $^3J_{H5-H4}$ = 10.3 Hz, $^3J_{H5-H6}$ = 3.3 Hz, 1 H, H^5); 4.47 (m, 1 H, H^2); 4.35−4.22 (m, 2 H, H^6); 3.99, 3.40, 3.38 (s, 6 H, NMe_2); 2.10−1.97 (s, 12 H, 4× O═CMe). Diastereomeric ratio = 1. ^{13}C{^{1}H} NMR (acetone-d_6): δ/ppm = 255.0 (μ-CO); 225.2 (C_α); 210.2 (CO); 200.0 (C_γ); 169.7, 169.5, 169.4, 169.1 (4× O═*C*Me); 96.8, 95.6 (C^1); 89.8, 89.7, 87.6, 87.4 (Cp); 80.5, 79.8 ($C_\gamma CH_2$); 70.9, 70.6 (C^5); 70.0, 69.9, 68.7 (C^3 + C^4); 68.1, 68.1 (C^2); 62.1, 61.9 (C^6); 50.7, 44.4 (NMe_2); 47.7, 47.1 (C_β); 19.9, 19.8, 19.7 (4× O═C*Me*) (Figure 10).

*[$Fe_2Cp_2(CO)(\mu$-CO)$\{\mu$-η^1:η^3-C_γ(CH_2O-2,3:4,5-Di-O-isopropylidene-)-β-D-fructopyranosyl)$C_\beta HC_\alpha NMe_2$}]CF_3SO_3, [**5a**]CF_3SO_3 (Figure 11).* From [**1′a**]CF_3SO_3, freshly prepared from [**1a**]CF_3SO_3 (218 mg, 0.41 mmol) and HC≡CCH_2OFru′ (147 mg, 0.49 mmol). Brown solid, yield 284 mg (86%). Anal. calcd for $C_{31}H_{38}F_3Fe_2NO_{11}S$: C, 46.46; H, 4.78; N, 1.75. Found: C, 46.32; H, 4.86; N, 1.70. HR-ESI-MS: $[M]^+$ m/z = 652.1286 (theoretical for $[C_{30}H_{38}Fe_2NO_8]^+$: m/z = 652.1296; error: −1.5 ppm). IR (CH_2Cl_2): $\tilde{\nu}$/cm^{-1} = 1991m (CO), 1810m (μ-CO), 1681w (C_αN). δ/ppm = 5.80−5.75 (m, 2 H, $C_\gamma CH_2$); 5.24, 5.24, 5.07, 5.06 (s, 10 H, Cp); 5.10, 5.03 (s, 1 H, C_βH); 4.69 (m, 1 H, H^4); 4.42 (m, 1 H, H^3); 4.30 (m, 1 H, H^5); 4.10−3.95 (m, 2 H, H^6); 3.98−3.93, 3.84−3.77 (m, 2 H, H^1); 3.88, 3.30, 3.30 (s, 6 H, NMe_2); 1.60, 1.59, 1.56, 1.53, 1.51, 1.40, 1.38 (s, 12 H, 2× CMe_2). Diastereomeric ratio = 1. ^{13}C{^{1}H} NMR ($CDCl_3$): δ/ppm = 256.2, 256.1 (μ-CO); 225.3, 225.1 (C_α); 209.8, 209.8 (CO); 201.7, 201.5 (C_γ); 109.1, 108.9, 108.8 (2× *C*Me$_2$); 102.6 (C^2); 89.4, 87.6 (Cp); 85.0, 84.9 ($C_\gamma CH_2$); 73.8, 73.6 (C^6); 71.0, 70.8, 70.7, 70.1 (C^3 + C^4 + C^5); 61.2 (C^1); 51.4, 44.9 (NMe_2); 50.1, 49.7 (C_β); 26.5, 26.1, 25.6, 24.1 (2× C*Me*$_2$) (Figure 11).

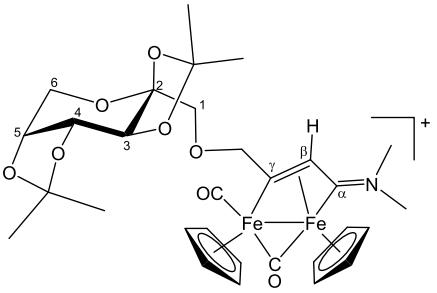

Figure 11. Structure of $[\mathbf{5a}]^+$.

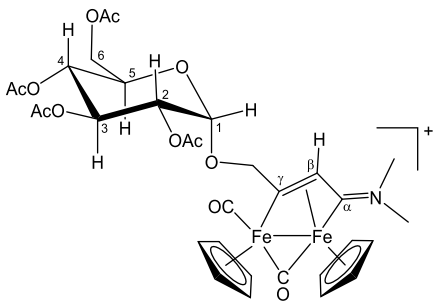

Figure 10. Structure of $[\mathbf{4}]^+$.

*[$Fe_2Cp_2(CO)(\mu$-CO)$\{\mu$-η^1:η^3-C_γ(CH_2O-2,3:4,5-Di-O-isopropylidene-)-β-D-fructopyranosyl)$C_\beta HC_\alpha N$(Me)(Xyl)}]CF_3SO_3, [**5b**]CF_3SO_3 (Figure 12).* From [**1′b**]CF_3SO_3, freshly prepared from [**1b**]CF_3SO_3 (229 mg, 0.37 mmol) and HC≡CCH_2OFru′ (135 mg, 0.45 mmol). Brown solid, yield 280 mg (85%). Anal. calcd for $C_{38}H_{44}F_3Fe_2NO_{11}S$: C, 51.19; H, 4.97; N, 1.57. Found: C, 50.94; H, 5.03; N, 1.47. HR-ESI-MS: $[M]^+$ m/z = 742.1759 (theoretical for $[C_{37}H_{44}Fe_2NO_8]^+$: m/z = 742.1766; error: −0.9 ppm). IR (CH_2Cl_2): $\tilde{\nu}$/cm^{-1} = 2002vs (CO), 1815s (μ-CO), 1633m (C_αN). ^{1}H NMR ($CDCl_3$): δ/ppm = 7.18, 7.10, 6.95 (m, 3 H, C_6H_3); 6.00−5.70 (m, 2 H, $C_\gamma CH_2$); 5.44, 5.21, 5.20 (s, 10 H, Cp); 4.71, 4.66 (s, 1 H, C_βH); 4.63 (m, 1 H, H^4); 4.30, 4.27 (m, 2 H, H^3 + H^5); 4.00−3.85 (m, 2 H, H^6); 3.95−3.85, 3.75 (m, 2 H, H^1); 4.20 (s, 3 H, NMe); 2.28, 2.27, 1.77 (s, 6 H, $C_6H_3Me_2$); 1.55, 1.54, 1.49, 1.45, 1.37, 1.36, 1.35, 1.31 (s, 12 H, 2× CMe_2). Diastereomeric ratio = 1. ^{13}C{^{1}H} NMR ($CDCl_3$): δ/ppm = 255.8, 253.9 (μ-CO); 232.9 (C_α); 209.9, 209.6 (CO); 205.8, 205.6 (C_γ); 145.9, 144.9, 131.4, 131.1 (*ipso*-C_6H_3); 129.6, 129.4, 129.3 (C_6H_3); 109.1, 108.6 (2× *C*Me$_2$); 102.6 (C^2); 90.3, 87.9 (Cp); 85.1, 84.7 ($C_\gamma CH_2$); 74.1, 73.5 (C^6); 70.9, 70.7, 70.1 (C^3 + C^4 + C^5); 61.1 (C^1); 48.8, 48.0 (C_β); 46.2, 46.1 (NMe); 26.5, 26.0, 25.6, 24.0 (2× C*Me*$_2$); 17.9, 17.2 ($C_6H_3Me_2$) (Figure 12).

General Procedure for the Synthesis of [6a−b]CF_3SO_3. A solution of [**1a−b**]CF_3SO_3 (ca. 0.5 mmol) in MeCN (ca. 10 mL) was

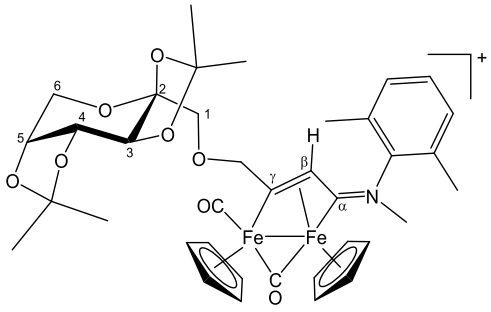

Figure 12. Structure of $[\mathbf{5b}]^+$.

https://doi.org/10.1021/acs.organomet.1c00519
Organometallics 2022, 41, 514−526

treated with Me_3NO (ca. 1.2 equiv). The resulting mixture was stirred for 50 min, and progressive color darkening was observed. The complete conversion of the starting material into the corresponding acetonitrile adduct [**1′a–b**]CF_3SO_3[36] was checked by IR spectroscopy. The volatiles were removed under vacuum to afford a dark-brown residue, which was dissolved in dichloromethane and treated with methyl propargyl ether. This solution was stirred at room temperature for 3 days, then it was charged on an alumina column. Elution with CH_2Cl_2/tetrahydrofuran (THF) mixtures allowed separation of the unreacted alkyne and impurities, and hence a brown band was collected with methanol. After removal of the solvent, the residue was dissolved in dichloromethane and filtered on a short celite pad. Evaporation of the solvent under vacuum afforded the product as a hygroscopic solid material.

*[$Fe_2Cp_2(CO)(\mu$-CO){μ-η^1:η^3-$C_\gamma(CH_2OMe)C_\beta HC_\alpha NMe_2$}]$CF_3SO_3$, [**6a**]$CF_3SO_3$ (Figure 13).* From [**1′a**]CF_3SO_3, freshly prepared from [**1a**]CF_3SO_3 (111 mg, 0.21 mmol) and methyl propargyl ether (0.17 mL, 2.0 mmol). Black solid, yield 114 mg (95%). Anal. calcd for $C_{20}H_{22}F_3Fe_2NO_6S$: C, 41.91; H, 3.87; N, 2.44. Found: C, 42.06; H, 3.74; N, 2.51. IR (CH_2Cl_2): $\tilde{\upsilon}$/cm^{-1} = 1990vs (CO), 1808s (μ-CO), 1681m (C_αN). ^{1}H NMR (acetone-d_6): δ/ppm = 5.99, 5.79 (d, 2 H, $^2J_{HH}$ = 11.7 Hz, CH_2); 5.52, 5.19 (s, 10 H, Cp); 5.09 (s, 1 H, C_βH); 3.94, 3.35 (s, 6 H, NMe_2); 3.74 (s, 3 H, OMe). ^{13}C{^{1}H} NMR (acetone-d_6): δ/ppm = 256.1 (μ-CO); 225.6 (C_α); 210.6 (CO); 202.8 (C_γ); 89.8, 87.6 (Cp); 85.3 (CH_2); 58.2 (OMe); 50.9, 44.6 (NMe_2); 47.9 (C_β) (Figure 13).

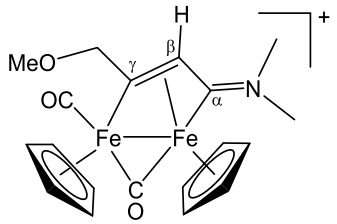

Figure 13. Structure of [**6a**]$^+$.

*[$Fe_2Cp_2(CO)(\mu$-CO){μ-η^1:η^3-$C_\gamma(CH_2OMe)C_\beta HC_\alpha N(Me)(Xyl)$}]$CF_3SO_3$, [**6b**]$CF_3SO_3$ (Figure 14).* From [**1′b**]CF_3SO_3, freshly prepared from [**1b**]CF_3SO_3 (79 mg, 0.13 mmol) and methyl propargyl ether (0.050 mL, 0.59 mmol). Dark-brown solid, yield 75 mg (88%). Anal. calcd for $C_{27}H_{28}F_3Fe_2NO_6S$: C, 48.89; H, 4.26; N, 2.11. Found: C, 48.99; H, 4.17; N, 2.17. IR (CH_2Cl_2): $\tilde{\upsilon}$/cm^{-1} = 2001vs (CO), 1814s (μ-CO), 1634m (C_αN), 1587w (C–C_{arom}). ^{1}H NMR ($CDCl_3$): δ/ppm = 7.17–7.09, 6.97–6.91 (m, 3 H, C_6H_3); 6.08, 5.53 (d, 2 H, $^2J_{HH}$ = 14 Hz, CH_2); 5.51, 5.27, 4.83 (s, 10 H, Cp); 4.68 (s, 1 H, C_βH); 4.20, 3.49 (s, 3 H, NMe); 3.67 (s, 3 H, OMe); 2.48, 2.28, 1.97, 1.75 (s, 6 H, $C_6H_3Me_2$). *E*/*Z* ratio = 11:1. ^{13}C{^{1}H} NMR ($CDCl_3$): δ/ppm = 254.7 (μ-CO); 233.4 (C_α); 209.8 (CO); 206.9 (C_γ); 144.9 (*ipso*-C_6H_3); 131.4, 131.2, 129.6, 129.4, 129.3 (C_6H_3); 90.4, 87.9 (Cp); 85.5 (CH_2); 59.0 (OMe); 47.3 (C_β); 46.3 (NMe); 18.2, 17.2 ($C_6H_3Me_2$) (Figure 14).

Behavior in Aqueous Media. *Solubility in D_2O.* The selected diiron compound was added to a D_2O solution (0.7 mL) of Me_2SO_2 (c = 7.1 × 10^{-3} mol·L^{-1}), and the resulting mixture was stirred at 21 °C for 30 min. The saturated solution was filtered to remove some solids, and then transferred into an NMR tube and analyzed by ^{1}H NMR spectroscopy. The concentration (i.e., solubility) was calculated by the relative integral with respect to Me_2SO_2 as internal standard [δ/ppm = 3.14 (s, 6 H) in D_2O)]. Solubility data are as follows. [**2**]CF_3SO_3: 6.5 × 10^{-3} M (6.1 g·L^{-1}); [**3a**]CF_3SO_3: 2.2 × 10^{-3} M (2.0 g·L^{-1});

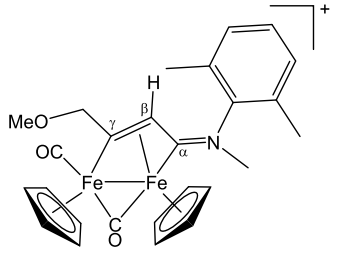

Figure 14. Structure of [**6b**]$^+$.

Stability in Aqueous Solution. The selected diiron compound (ca. 4 mg) was added to 1 mL of D_2O/DMSO-d_6 containing Me_2SO_2 (3.36 × 10^{-3} M), and the resulting mixture was stirred at ambient temperature for 30 min. The final mixture was filtered over celite, and the filtered solution was transferred into an NMR tube. The solution was analyzed by ^{1}H NMR ("time0") and subsequently heated at 37 °C for 72 h. After cooling to room temperature, the final solution was separated from a brown solid by filtration through celite, and the ^{1}H NMR spectrum was recorded (delay time = 3 s; number of scans = 20). In each case, no new {FeCp} species was identified. The amount of starting material in solution (% with respect to the initial spectrum) was calculated by the relative integral with respect to Me_2SO_2 as the internal standard (δ/ppm = 3.14 (s, 6 H)), Table 1.[37] NMR spectra at time0 were as follows.

[**2**]CF_3SO_3: ^{1}H NMR (D_2O): δ/ppm = 6.30–5.70 (m, 2 H, $C_\gamma CH_2$); 5.31, 4.97 (s, 10 H, Cp); 3.73, 3.16 (s, 6 H, NMe_2).

[**3a**]CF_3SO_3: ^{1}H NMR (D_2O): δ/ppm = 6.10–5.80 (m, 2 H, $C_\gamma CH_2$); 5.32, 5.00 (s, 10 H, Cp); 3.74, *3.18*, 3.17 (s, 6 H, NMe_2); 2.18, *2.16*, 2.10, 2.06, 2.03, 1.99, 1.98 (s, 12 H, 4× O=CMe).

[**3b**]CF_3SO_3: ^{1}H NMR (DMSO-d_6/D_2O = 1:2): δ/ppm = 7.30–7.00 (m, 3 H, C_6H_3); 6.10–5.80 (m, 2 H, $C_\gamma CH_2$); 5.58, 5.54, 5.28, 5.27 (s, 10 H, Cp); 4.20, 4.19 (s, 3 H, NMe); 2.26, 2.25, 1.79, 1.78 (s, 6 H, $C_6H_3Me_2$); 2.20, 2.19, 2.13, 2.10, 2.06, 2.04, 2.03, 2.00 (s, 12 H, 4× O=CMe).

[**4**]CF_3SO_3: ^{1}H NMR (DMSO-d_6/D_2O = 1:2): δ/ppm = 6.10–5.75 (m, 2 H, $C_\gamma CH_2$); 5.41, 5.38, 5.09 (s, 10 H, Cp); 3.80, 3.24, 3.22 (s, 6 H, NMe_2); 2.15–2.00 (s, 12 H, 4× O=CMe).

[**5a**]CF_3SO_3: ^{1}H NMR (DMSO-d_6/D_2O = 1:2): δ/ppm = 6.00–5.70 (m, 2 H, $C_\gamma CH_2$); 5.35, 5.35, 5.02 (s, 10 H, Cp); 3.74, 3.16 (s, 6 H, NMe_2); 1.55, 1.54, 1.46, 1.45, 1.44, 1.43, 1.35, 1.33 (s, 12 H, 2× CMe_2).

[**5b**]CF_3SO_3: ^{1}H NMR (DMSO-d_6/D_2O = 1:2): δ/ppm = 7.30–6.90 (m, 3 H, C_6H_3); 6.00–5.60 (m, 2 H, $C_\gamma CH_2$); 5.49, 5.48, 5.20 (s, 10 H, Cp); 4.13 (s, 3 H, NMe); 2.20, 1.72 (s, 6 H, $C_6H_3Me_2$); 1.49, 1.42, 1.35, 1.34, 1.30, 1.22, 1.18 (s, 12 H, 2× CMe_2).

[**6a**]CF_3SO_3: ^{1}H NMR (DMSO-d_6/D_2O = 1:2): δ/ppm = 5.68 (m, 2 H, $C_\gamma CH_2$); 5.34, 5.00 (s, 10 H, Cp); 4.82 (s, 1 H, C_βH); 3.73, 3.16 (s, 6 H, NMe_2); 3.67 (s, 3 H, OMe).

[**6b**]CF_3SO_3: ^{1}H NMR (DMSO-d_6/D_2O = 1:2): δ/ppm = 7.30–6.90 (m, 3 H, C_6H_3); 5.80–5.50 (m, 2 H, $C_\gamma CH_2$); 5.47, 5.19 (s, 10 H, Cp); 4.48 (s, 1 H, C_βH); 4.13 (s, 3 H, NMe); 3.54 (s, 3 H, OMe); 2.19, 1.73 (s, 6 H, $C_6H_3Me_2$).

Stability in Cell Culture Medium. The selected diiron compound (ca. 3 mg) was dissolved in DMSO (0.2 mL) in a glass tube, and then 4 mL of RPMI-1640 medium (Merck; modified with sodium bicarbonate, without L-glutamine and phenol red, liquid, sterile-filtered, suitable for cell culture) was added. A portion of the resulting solution was diluted 1:1000 with acetonitrile, filtered on a poly(tetrafluoroethylene) (PTFE) filter (0.45 μm pore size), and analyzed by flow injection ESI-MS (time0), while the remaining solution was kept at 37 °C for 72 h and stored in the dark. Then, the final mixture was diluted 1:1000 with acetonitrile, filtered on a PTFE filter (0.45 μm pore size), and analyzed by flow injection ESI-MS (injection volume = 0.1–1 μL, depending on the instrumental response; eluent = acetonitrile). The amount of unaltered complex in solution (% with respect to the time0 mass spectrum) was calculated as the ratio between the intensity of the corresponding molecular ions, Table 1. Assuming a comparable ionizability for diiron vinyliminium complexes (with or without the sugar moiety), the overall percentage of all diiron species in solution, compared to the starting complex at time0, is also provided. Mass spectra after 72 h are displayed in Figures S43–S50 and are as follows.

https://doi.org/10.1021/acs.organomet.1c00519
Organometallics 2022, 41, 514–526

[**2**]CF_3SO_3: [**6a**]$^+$ (m/z calcd for $[C_{19}H_{22}Fe_2NO_3]^+$ 424.0299, found 424.0296, error: −0.7 ppm) + [**9a**]$^+$ (m/z calcd for $[C_{18}H_{20}Fe_2NO_3]^+$ 410.0142, found 410.0137, error: −1.2 ppm), ratio [**6a**]$^+$:[**9a**]$^+$ = 55:1.

[**3a**]CF_3SO_3: [**3a**]$^+$ (m/z calcd for $[C_{32}H_{38}Fe_2NO_{12}]^+$ 740.1094, found 740.1087, error: −0.9 ppm) + [**3a-Ac+H**]$^+$ (m/z calcd for $[C_{30}H_{36}Fe_2NO_{11}]^+$ 698.0988, found 698.0975, error: −1.8 ppm) + [**3a-2Ac+2H**]$^+$ (m/z calcd for $[C_{28}H_{34}Fe_2NO_{10}]^+$ 656.0883, found 656.0871, error: −1.8 ppm), ratio [**3a**]$^+$:[**3a-Ac+H**]$^+$:[**3a-2Ac+2H**]$^+$ = 56:11:1.

[**3b**]CF_3SO_3: [**3b**]$^+$ (m/z calcd for $[C_{39}H_{44}Fe_2NO_{12}]^+$ 830.1564, found 830.1570, error: 0.7 ppm) + [**3b-Ac+H**]$^+$ (m/z calcd for $[C_{37}H_{42}Fe_2NO_{11}]^+$ 788.1458, found 788.1459, error: 0.1 ppm) + [**3b-2Ac+2H**]$^+$ (m/z calcd for $[C_{35}H_{40}Fe_2NO_{10}]^+$ 746.1352, found 746.1353, error: 0.1 ppm), ratio [**3b**]$^+$:[**3b-Ac+H**]$^+$:[**3b-2Ac+2H**]$^+$ = 11:3:1.

[**4**]CF_3SO_3: [**4**]$^+$ (m/z calcd for $[C_{32}H_{38}Fe_2NO_{12}]^+$ 740.1094, found 740.1099, error: 0.7 ppm) + [**4-Ac+H**]$^+$ (m/z calcd for $[C_{30}H_{36}Fe_2NO_{11}]^+$ 698.0988, found 698.0991, error: 0.4 ppm) + [**4-2Ac+2H**]$^+$ (m/z calcd for $[C_{28}H_{34}Fe_2NO_{10}]^+$ 656.0883, found 656.0895, error: 1.8 ppm), ratio [**4**]$^+$:[**4-Ac+H**]$^+$:[**4-2Ac+2H**]$^+$ = 4:2:1.

[**5a**]CF_3SO_3: [**5a**]$^+$ (m/z calcd for $[C_{30}H_{38}Fe_2NO_8]^+$ 652.1297, found 652.1300, error: 0.5 ppm).

[**5b**]CF_3SO_3: [**5b**]$^+$ (m/z calcd for $[C_{37}H_{44}Fe_2NO_8]^+$ 742.1767, found 742.1778, error: 1.5 ppm).

[**6a**]CF_3SO_3: [**6a**]$^+$ (m/z calcd for $[C_{19}H_{22}Fe_2NO_3]^+$ 424.0299, found 424.0293, error: −1.4 ppm) + [**9a**]$^+$ (m/z calcd for $[C_{18}H_{20}Fe_2NO_3]^+$ 410.0142, found 410.0128, error: −3.4 ppm), ratio [**6a**]$^+$:[**9a**]$^+$ = 55:1.

[**6b**]CF_3SO_3: [**6b**]$^+$ (m/z calcd for $[C_{26}H_{28}Fe_2NO_3]^+$ 514.0769, found 514.0775, error: 1.2 ppm).

All of the isotopic patterns fit well the corresponding calculated ones.

Determination of Partition Coefficients (Log P_{ow}). Partition coefficients (P_{ow}; IUPAC: K_D partition constant,[38] defined as $P_{ow} = c_{org}/c_{aq}$, where c_{org} and c_{aq} are the molar concentrations of the selected compound in the organic and aqueous phases, respectively, were determined by the shake-flask method and UV−vis measurements.[37,39] Values of Log P_{ow} for diiron complexes are compiled in Table 2. All of the operations were carried out at 21 ± 1 °C. Deionized water and 1-octanol were mixed and vigorously stirred for 24 h at ambient temperature to allow saturation of both phases, then separated by centrifugation, and used for the following experiments. A solution of the selected diiron compound in octanol-saturated water (V = 5 mL) was prepared and its UV−vis spectrum was recorded. An aliquot of the solution (V_{aq} = 1.5 mL) was then transferred into a test tube and the organic phase ($V_{org} = V_{aq}$ = 1.5 mL) was added. The mixture was vigorously stirred for 20 min, and the resulting emulsion was centrifuged (5000 rpm, 10′). Hence, the UV−vis spectrum of the aqueous phase was recorded. The procedure was repeated three times for each compound. The partition coefficient was then calculated as $P_{ow} = \frac{A_{0,aq} - A_{aq}}{A_{aq}}$, where $A_{0,aq}$ and A_{aq} are the absorbance values in the aqueous phase, respectively, before and after partition with the organic phase.[39] For [**6b**]CF_3SO_3, an inverse procedure was followed, starting from a solution of the compound in water-saturated octanol. The partition coefficient was calculated as $P_{ow} = A_{org}/(A_{org}{}^0 - A_{org})$ where $A_{org}{}^0$ and A_{org} are the absorbances in the organic phase, respectively, before and after partition with the aqueous phase. UV−vis measurements were carried out using 1 cm PMMA cuvettes. The wavelength of the maximum absorption of each compound (415−400 nm range) was used for UV−vis quantification.

Cell Culture and Cytotoxicity Studies. *Assessment of Cytotoxic Activity.* CT26 (mouse colon carcinoma) and MCF-7 (human breast adenocarcinoma) cells were cultured in DMEM, U87 (human glioblastoma) cells were cultured in MEM, and RPE-1 (human normal retina pigmented epithelium) cells were cultured in DMEM/F-12 media (Gibco). All of the culture media were supplemented with 10% fetal calf serum (Gibco) and 1% PenStrep (Gibco). Cells were maintained in a humidified atmosphere at 37°C and 5% CO_2.

Cells were seeded at a 4.000 cells/well density in flat-bottom 96-well plates (100 μL/well) and were incubated at 37°C for 24 h to allow the cells to attach to the bottom of the wells. Stock solutions of the diiron compounds were prepared in DMSO and rapidly diluted in a medium (1% DMSO content maximum). The stock solution of the reference drug cisplatin was prepared in saline solution, NaCl 0.9% w/v. The medium was replaced by dilutions of tested compounds in a fresh medium (100 μL/well) to obtain the following concentration range: 0.01, 0.03, 0.1, 0.3, 1, 3, 10, 30, and 100 μM for the tested compounds and 0.3, 0.6, 2, 3, 6, 10, and 30 μM for the reference drug cisplatin. After loading the drug, cells were incubated for 48 h at 37 °C. The medium was then replaced with 100 μL of a fresh medium containing resazurin (0.2 mg $mL^{-1)}$ and incubated for 4 h. The florescence of the wells, directly proportional to the number of survived cells, was determined by reading the plates using a SpectraMaxM2 Microplate Reader (λ_{exc} = 540 nm; λ_{read} = 590 nm). Fluorescence data were normalized by attributing 100% cell viability to the mean signal obtained for the lowest compound concentration and 0% to the signal obtained from wells containing the highest drug concentration or only the resazurin solution (when no toxicity was observed). Data were fitted using GraphPad Prism Software (v6) and IC_{50} values were calculated by nonlinear regression. All experiments were performed in triplicates.

Viability Test With No-Glucose Medium. CT26 cells were seeded at a 4.000 cells/well density in flat-bottom 96-well plates (100 μL/well) and were incubated at 37 °C for 8 h to allow the attachment of cells to the bottom of the wells. After 8 h, the medium was carefully removed and replaced with no-glucose DMEM. The cells were incubated overnight. Stock solutions of the compounds were prepared in DMSO and rapidly diluted in a medium without glucose (1% DMSO content maximum). The medium was replaced by dilutions of tested compounds in a fresh no-glucose medium (100 μL/well) to obtain the following concentration ranges: 0.3, 1, 3, 10, 30, and 100 μM for the tested compounds and 0.03, 0.1, 0,3, 1, 3, and 30 μM for the reference drug cisplatin. After loading the drug, the cells were incubated for 48 h at 37 °C. The medium was then replaced with 100 μL/well of a fresh medium containing resazurin (0.2 mg mL^{-1}) and incubated for 4 h. The fluorescence of the wells, directly proportional to the number of survived cells, was determined by reading the plates using a SpectraMaxM2 Microplate Reader (λ_{exc} = 540 nm; λ_{read} = 590 nm). Fluorescence data were normalized by attributing 100% cell viability to the mean signal obtained for the lowest compound concentration and 0% to the signal obtained from wells containing the highest drug concentration or only the resazurin solution (when no toxicity was observed). Data were fitted using GraphPad Prism Software (v6), and IC_{50} values were calculated by nonlinear regression. All experiments were performed in triplicates.

Scratch Assay. CT26 cells were seeded at 2 × 10^5 cells/well density in a 6-well plate. The cells were incubated for 48 h to obtain a 90−100% confluency. The cellular monolayer was scratched with a 200 μL tip, the cells were washed once with PBS to remove the debris, and then 4 mL of the solution containing IC_{20} of each tested drug was added to the wells. Less than 1% of DMSO was used in the preparation of the drug solutions. The cells were monitored by imaging over 30 h with the following time intervals: 1, 3, 8, 24, 30 h. Agilent BioTek Gen 5 Cytation was used to record the pictures. The cells were maintained at 37 °C during the time needed for the imaging. The images are representative from one successive experiment out of three successive individual experiments.

■ ASSOCIATED CONTENT

Supporting Information

The Supporting Information is available free of charge at https://pubs.acs.org/doi/10.1021/acs.organomet.1c00519.

Synthesis and ^{1}H NMR characterization of carbohydrate alkynes (Figures S1−S4 and S5−S8); IR spectra (Figures S9−S17); NMR spectra (Figures S18−S42);

https://doi.org/10.1021/acs.organomet.1c00519
Organometallics 2022, 41, 514−526

ESI-MS spectra (Figures S43−S50); and dose−response cell viability curves (Figures S51−S55) (PDF)

AUTHOR INFORMATION

Corresponding Authors

Gilles Gasser − *Chimie ParisTech, PSL University, CNRS, Institute of Chemistry for Life and Health Sciences, 75005 Paris, France;* orcid.org/0000-0002-4244-5097; Email: gilles.gasser@chimieparistech.psl.eu

Valeria Di Bussolo − *Department of Pharmacy, University of Pisa, 56126 Pisa, Italy*; Email: valeria.dibussolo@unipi.it

Fabio Marchetti − *Department of Chemistry and Industrial Chemistry, University of Pisa, 56124 Pisa, Italy;* orcid.org/0000-0002-3683-8708; Email: fabio.marchetti1974@unipi.it

Authors

Silvia Schoch − *Department of Chemistry and Industrial Chemistry, University of Pisa, 56124 Pisa, Italy*

Dalila Iacopini − *Department of Chemistry and Industrial Chemistry, University of Pisa, 56124 Pisa, Italy*

Maria Dalla Pozza − *Chimie ParisTech, PSL University, CNRS, Institute of Chemistry for Life and Health Sciences, 75005 Paris, France*

Sebastiano Di Pietro − *Department of Pharmacy, University of Pisa, 56126 Pisa, Italy*

Ilaria Degano − *Department of Chemistry and Industrial Chemistry, University of Pisa, 56124 Pisa, Italy;* orcid.org/0000-0002-3585-8555

Complete contact information is available at: https://pubs.acs.org/10.1021/acs.organomet.1c00519

Author Contributions

[‖]S.S., D.I., and M.D.P. contributed equally to this work.

Notes

The authors declare no competing financial interest.

ACKNOWLEDGMENTS

The authors are grateful for financial support from the European Union's Horizon 2020 Research and Innovation Program (Marie Skłodowska−Curie grant agreement no. 861381), the ERC Consolidator Grant PhotoMedMet to G.G. (GA 681679), the program "Investissements d′ Avenir" launched by the French Government and implemented by the ANR with the reference ANR-10-IDEX-0001-02 PSL (G.G.), and the University of Pisa (PRA_2020_39 "New horizons in CO_2 chemistry: from capture to fine chemicals and metal-based drugs" and PRA_2020_58 "Agenti innovativi e nano-sistemi per target molecolari nell′ambito dell′oncologia di precisione"). The authors also thank Dr. Robin Vinck for his precious support and help during the cytotoxicity experiments.

REFERENCES

(1) Selected recent reviews (a) Murray, B. S.; Dyson, P. J. Recent progress in the development of organometallics for the treatment of cancer. *Curr. Opin. Chem. Biol.* **2020**, *56*, 28−34. (b) Anthony, E. J.; Bolitho, E. M.; Bridgewater, H. E.; Carter, O. W. L.; Donnelly, J. M.; Imberti, C.; Lant, E. C.; Lermyte, F.; Needham, R. J.; Palau, M.; Sadler, P. J.; Shi, H.; Wang, F.-X.; Zhang, W.-Y.; Zhang, Z. Metallodrugs are unique: opportunities and challenges of discovery and development. *Chem. Sci.* **2020**, *11*, 12888−12917. (c) Boros, E.; Dyson, P. J.; Gasser, G. Classification of Metal-based Drugs According to Their Mechanisms of Action. *Chem* **2020**, *6*, 41−60. (d) Soldevila-Barreda, J. J.; Metzler-Nolte, N. Intracellular Catalysis with Selected Metal Complexes and Metallic Nanoparticles: Advances toward the Development of Catalytic Metallodrugs. *Chem. Rev.* **2019**, *119*, 829−869.

(2) (a) Oun, R.; Moussa, Y. E.; Wheate, N. J. The side effects of platinum-based chemotherapy drugs: a review for chemists. *Dalton Trans.* **2018**, *47*, 6645−6653. (b) Siddik, Z. H. Cisplatin: mode of cytotoxic action and molecular basis of resistance. *Oncogene* **2003**, *22*, 7265−7279. (c) Apps, M. G.; Choi, E. H. Y.; Wheate, N. J. The state-of-play and future of platinum drugs. *Endocr.-Relat. Cancer* **2015**, *22*, R219−R233.

(3) (a) Basu, U.; Roy, M.; Chakravarty, A. R. Recent advances in the chemistry of iron-based chemotherapeutic agents. *Coord. Chem. Rev.* **2020**, *417*, No. 213339. (b) Patra, M.; Gasser, G. The medicinal chemistry of ferrocene and its derivatives. *Nat. Rev. Chem.* **2017**, *1*, No. 0066. (c) Muenzner, J. K.; Biersack, B.; Albrecht, A.; Rehm, T.; Lacher, U.; Milius, W.; Casini, A.; Zhang, J.-J.; Ott, I.; Brabec, V.; Stuchlikova, O.; Andronache, I. C.; Kaps, L.; Schuppan, D.; Schobert, R. Ferrocenyl-Coupled N-Heterocyclic Carbene Complexes of Gold(I): A Successful Approach to Multinuclear Anticancer Drugs. *Chem. - Eur. J.* **2016**, *22*, 18953−18962.

(4) (a) Jaouen, G.; Vessieres, A.; Top, S. Ferrocifen type anti cancer drugs. *Chem. Soc. Rev.* **2015**, *44*, 8802−8817. (b) Gasser, G.; Ott, I.; Metzler-Nolte, N. Organometallic Anticancer Compounds. *J. Med. Chem.* **2011**, *54*, 3−25.

(5) (a) Wang, Y.; Dansette, P. M.; Pigeon, P.; Top, S.; McGlinchey, M. J.; Mansuy, D.; Jaouen, G. A new generation of ferrociphenols leads to a great diversity of reactive metabolites, and exhibits remarkable antiproliferative properties. *Chem. Sci.* **2018**, *9*, 70−78. (b) Leonidova, A.; Anstaett, P.; Pierroz, V.; Mari, C.; Spingler, B.; Ferrari, S.; Gasser, G. Induction of Cytotoxicity through Photorelease of Aminoferrocene. *Inorg. Chem.* **2015**, *54*, 9740−9748. (c) Ocasio, C. A.; Sansook, S.; Jones, R.; Roberts, J. M.; Scott, T. G.; Tsoureas, N.; Coxhead, P.; Guille, M.; Tizzard, G. J.; Coles, S. J.; Hochegger, H.; Bradner, J. E.; Spencer, J. Pojamide: An HDAC3-Selective Ferrocene Analogue with Remarkably Enhanced Redox-Triggered Ferrocenium Activity in Cells. *Organometallics* **2017**, *36*, 3276−3283.

(6) (a) BenYosef, D.; Romano, D.; Hadiji, M.; Dyson, P. J.; Blom, B. Facile synthesis of heterobimetallic [Fe^{II}(μ-diphosphine)Ru^{II}] and homobimetallic [Fe^{II}(μ-diphosphine)Fe^{II}] complexes and their in vitro cytotoxic activity on cisplatin-resistant cancer cells. *Inorg. Chim. Acta* **2020**, *510*, No. 119731. (b) Pilon, A.; Brás, A. R.; Côrte-Real, L.; Avecilla, F.; Costa, P. J.; Preto, A.; Garcia, M. H.; Valente, A. A New Family of Iron(II)-Cyclopentadienyl Compounds Shows Strong Activity against Colorectal and Triple Negative Breast Cancer Cells. *Molecules* **2020**, *25*, No. 1592.

(7) Agonigi, G.; Biancalana, L.; Lupo, M. G.; Montopoli, M.; Ferri, N.; Zacchini, S.; Binacchi, F.; Biver, T.; Campanella, B.; Pampaloni, G.; Zanotti, V.; Marchetti, F. Exploring the Anticancer Potential of Diiron Bis-cyclopentadienyl Complexes with Bridging Hydrocarbyl Ligands: Behavior in Aqueous Media and *In Vitro* Cytotoxicity. *Organometallics* **2020**, *39*, 645−657.

(8) (a) Swanson, K. D.; Ortillo, D. O.; Broderick, J. B.; Peters, J. W. *Encyclopedia of Inorganic and Bioinorganic Chemistry*, 2nd ed.; Wiley, 2011. (b) Land, H.; Senger, M.; Berggren, G.; Stripp, S. T. Current State of [FeFe]-Hydrogenase Research: Biodiversity and Spectroscopic Investigations. *ACS Catal.* **2020**, *10*, 7069−7086.

(9) See for instance (a) Ritleng, V.; Chetcuti, M. J. Hydrocarbyl Ligand Transformations on Heterobimetallic Complexes. *Chem. Rev.* **2007**, *107*, 797−858. (b) Adams, R. D.; Captain, B. Bimetallic cluster complexes: synthesis, structures and applications to catalysis. *J. Organomet. Chem.* **2004**, *689*, 4521−4529.

(10) See for instance (a) Mazzoni, R.; Salmi, M.; Zanotti, V. C-C Bond Formation in Diiron Complexes. *Chem. - Eur. J.* **2012**, *18*, 10174−10194. (b) Casey, C. P.; Austin, E. A. Photochemical Reactions of Diiron μ-Alkenylidene Complexes with Hydrogen, Trialkylsilanes, and Diazo Compounds: Cleavage to Alkenes, Vinylsilanes, and Allenes. *J. Am. Chem. Soc.* **1988**, *110*, 7106−7113.

(11) Marchetti, F. Constructing Organometallic Architectures from Aminoalkylidyne Diiron Complexes. *Eur. J. Inorg. Chem.* **2018**, *2018*, 3987−4003.
(12) Agonigi, G.; Bortoluzzi, M.; Marchetti, F.; Pampaloni, G.; Zacchini, S.; Zanotti, V. Regioselective Nucleophilic Additions to Diiron Carbonyl Complexes Containing a Bridging Aminocarbyne Ligand: A Synthetic, Crystallographic and DFT Study. *Eur. J. Inorg. Chem.* **2018**, *2018*, 960−971.
(13) Ciancaleoni, G.; Zacchini, S.; Zanotti, V.; Marchetti, F. DFT Mechanistic Insights into the Alkyne Insertion Reaction Affording Diiron μ-Vinyliminium Complexes and New Functionalization Pathways. *Organometallics* **2018**, *37*, 3718−3731.
(14) Biancalana, L.; De Franco, M.; Ciancaleoni, G.; Zacchini, S.; Pampaloni, G.; Gandin, V.; Marchetti, F. Easily Available, Amphiphilic Diiron Cyclopentadienyl Complexes Exhibit in Vitro Anticancer Activity in 2D and 3D Human Cancer Cells through Redox Modulation Triggered by CO Release. *Chem. - Eur. J.* **2021**, *27*, 10169−10185.
(15) (a) Rocco, D.; Batchelor, L. K.; Agonigi, G.; Braccini, S.; Chiellini, F.; Schoch, S.; Biver, T.; Funaioli, T.; Zacchini, S.; Biancalana, L.; Ruggeri, M.; Pampaloni, G.; Dyson, P. J.; Marchetti, F. Anticancer Potential of Diiron Vinyliminium Complexes. *Chem. - Eur. J.* **2019**, *25*, 14801−14816. (b) Agonigi, G.; Batchelor, L. K.; Ferretti, E.; Schoch, S.; Bortoluzzi, M.; Braccini, S.; Chiellini, F.; Biancalana, L.; Zacchini, S.; Pampaloni, G.; Sarkar, B.; Dyson, P. J. Mono-, Di- and Tetra-iron Complexes with Selenium or Sulphur Functionalized Vinyliminium Ligands: Synthesis, Structural Characterization and Antiproliferative Activity. *Molecules* **2020**, *25*, No. 1656. (c) Braccini, S.; Rizzi, G.; Biancalana, L.; Pratesi, A.; Zacchini, S.; Pampaloni, G.; Chiellini, F.; Marchetti, F. Anticancer Diiron Vinyliminium Complexes: A Structure−Activity Relationship Study. *Pharmaceutics* **2021**, *13*, No. 1158.
(16) (a) Štarha, P.; Trávníček, Z. Non-platinum complexes containing releasable biologically active ligands. *Coord. Chem. Rev.* **2019**, *395*, 130−145. (b) Tremlett, W. D. J.; Goodman, D. M.; Steel, T. R.; Kumar, S.; Wieczorek-Blauz, A.; Walsh, F. P.; Sullivan, M. P.; Matthew, P.; Hanif, M.; Hartinger, C. G. Design concepts of half-sandwich organoruthenium anticancer agents based on bidentate bioactive ligands. *Coord. Chem. Rev.* **2021**, *445*, No. 213950. (c) Chellan, P.; Sadler, P. J. Enhancing the Activity of Drugs by Conjugation to Organometallic Fragments. *Chem. - Eur. J.* **2020**, *26*, 8676−8688. (d) Golbaghi, G.; Castonguay, A. Rationally Designed Ruthenium Complexes for Breast Cancer Therapy. *Molecules* **2020**, *25*, No. 265.
(17) Schoch, S.; Hadiji, M.; Pereira, S. A. P.; Saraiva, M. L. M. F. S.; Braccini, S.; Chiellini, F.; Biver, T.; Zacchini, S.; Pampaloni, G.; Dyson, P. J.; Marchetti, F. A Strategy to Conjugate Bioactive Fragments to Cytotoxic Diiron Bis(cyclopentadienyl) Complexes. *Organometallics* **2021**, *40*, 2516−2528.
(18) (a) Warburg, O. On the origin of cancer cells. *Science* **1956**, *123*, 309−314. (b) Calvaresi, E. C.; Hergenrother, P. J. Glucose conjugation for the specific targeting and treatment of cancer. *Chem. Sci.* **2013**, *4*, 2319−2333. (c) Granchi, C.; Minutolo, F. Anticancer agents that counteract tumor glycolysis. *ChemMedChem* **2012**, *7*, 1318−1350. (d) Jiang, H.; Qin, X.; Wang, Q.; Xu, Q.; Wang, J.; Wu, Y.; Chen, W.; Wang, C.; Zhang, T.; Xing, D.; Zhang, R. Application of carbohydrates in approved small molecule drugs: A review. *Eur. J. Med. Chem.* **2021**, *223*, No. 113633.
(19) Tanasova, M.; Joseph, R. F. Molecular Tools for Facilitative Carbohydrate Transporters (Gluts). *ChemBioChem* **2017**, *18*, 1774−1788.
(20) (a) Ma, J.; Wang, Q.; Huang, Z.; Yang, Z.; Nie, Q.; Hao, W.; Wang, P. G.; Wang, X. Glycosylated Platinum(IV) Complexes as Substrates for Glucose Transporters (GLUTs) and Organic Cation Transporters (OCTs) Exhibited Cancer Targeting and Human Serum Albumin Binding Properties for Drug Delivery. *J. Med. Chem.* **2017**, *60*, 5736−5748. (b) Annunziata, A.; Liberti, D.; Bedini, E.; Cucciolito, M. E.; Loreto, D.; Monti, D. M.; Merlino, A.; Ruffo, F. Square-Planar vs. Trigonal Bipyramidal Geometry in Pt (II) Complexes Containing Triazole-Based Glucose Ligands as Potential Anticancer Agents. *Int. J. Mol. Sci.* **2021**, *22*, No. 8704.
(21) (a) Bononi, G.; Iacopini, D.; Cicio, G.; Di Pietro, S.; Granchi, C.; Di Bussolo, V.; Minutolo, F. Glycoconjugated Metal Complexes as Cancer Diagnostic and Therapeutic Agents. *ChemMedChem* **2021**, *16*, 30−64. (b) Pröhl, M.; Moser, P. D.; Czaplewska, J. A.; Hoffmann, P.; Buś, T.; Traeger, A.; Goerls, H.; Schubert, U. S.; Gottschaldt, M. Synthesis of D-fructose conjugated ligands via C6 and C1 and their corresponding $[Ru(bpy)_2(L)]Cl_2$ complexes. *Carbohydr. Res.* **2017**, *446*−*447*, 19−27. (c) Pettenuzzo, A.; Montagner, D.; McArdle, P.; Ronconi, L. An innovative and efficient route to the synthesis of metal-based glycoconjugates: proof-of-concept and potential applications. *Dalton Trans.* **2018**, *47*, 10721−10736. (d) Hartinger, C. G.; Nazarov, A. A.; Ashraf, S. M.; Dyson, P. J.; Keppler, B. K. Carbohydrate-Metal Complexes and their Potential as Anticancer Agents. *Curr. Med. Chem.* **2008**, *15*, 2574−2591. (e) Storr, T.; Thompson, K. H.; Orvig, C. Design of targeting ligands in medicinal inorganic chemistry. *Chem. Soc. Rev.* **2006**, *35*, 534−544. (f) Ott, I.; Koch, T.; Shorafa, H.; Bai, Z.; Poeckel, D.; Steinhilber, D.; Gust, R. Synthesis, cytotoxicity, cellular uptake and influence on eicosanoid metabolism of cobalt−alkyne modified fructoses in comparison to auranofin and the cytotoxic COX inhibitor Co-ASS. *Org. Biomol. Chem.* **2005**, *3*, 2282−2286.
(22) Gonzalez, P. S.; O'Prey, J.; Cardaci, S.; Barthet, V. G. A.; Sakamaki, J.-i.; Beaumatin, F.; Roseweir, A.; Gay, D. M.; Mackay, G.; Malviya, G.; Kania, E.; Ritchie, S.; Baudot, A. D.; Zunino, B.; Mrowinska, A.; Nixon, C.; Ennis, D.; Hoyle, A.; Millan, D.; McNeish, I. A.; Sansom, O. J.; Edwards, J.; Ryan, K. M. Mannose impairs tumour growth and enhances chemotherapy. *Nature* **2018**, *563*, 719−723.
(23) (a) Basu, U.; Khan, I.; Hussain, A.; Gole, B.; Kondaiah, P.; Chakravarty, A. R. Carbohydrate-Appended Tumor Targeting Iron(III) Complexes Showing Photocytotoxicity in Red Light. *Inorg. Chem.* **2014**, *53*, 2152−2162. (b) Florindo, P. R.; Pereira, D. M.; Borralho, P. M.; Rodrigues, C. M. P.; Piedade, M. F. M.; Fernandes, A. C. Cyclopentadienyl−Ruthenium(II) and Iron(II) Organometallic Compounds with Carbohydrate Derivative Ligands as Good Colorectal Anticancer Agents. *J. Med. Chem.* **2015**, *58*, 4339−4347. (c) Song, H.; Allison, S. J.; Brabec, V.; Bridgewater, H. E.; Kasparkova, J.; Kostrhunova, H.; Novohradsky, V.; Phillips, R. M.; Pracharova, J.; Rogers, N. J.; Shepherd, S. L.; Scott, P. Glycoconjugated Metallohelices have Improved Nuclear Delivery and Suppress Tumour Growth In Vivo. *Angew. Chem., Int. Ed.* **2020**, *59*, 14677−14685.
(24) Roy, B.; Mukhopadhyay, B. Sulfuric acid immobilized on silica: an excellent catalyst for Fischer type glycosylation. *Tetrahedron Lett.* **2007**, *48*, 3783−3787.
(25) Hausherr, A.; Orschel, B.; Scherer, S.; Reissig, H.-U. Synthesis of Enantiopure 1-Alkoxyallenes and their 3-Alkylated Derivatives. *Synthesis* **2001**, *2001*, 1377−1385.
(26) (a) Albano, V. G.; Busetto, L.; Marchetti, F.; Monari, M.; Zacchini, S.; Zanotti, V. Diiron μ-Vinyliminium Complexes from Acetylene Insertion into a Metal−Aminocarbyne Bond. *Organometallics* **2003**, *22*, 1326−1331. (b) Albano, V. G.; Busetto, L.; Marchetti, F.; Monari, M.; Zacchini, S.; Zanotti, V. Stereochemistry of the insertion of disubstituted alkynes into the metal aminocarbyne bond in diiron complexes. *J. Organomet. Chem.* **2004**, *689*, 528−538.
(27) (a) Marchetti, F.; Zacchini, S.; Zanotti, V. Photochemical Alkyne Insertions into the Iron−Thiocarbonyl Bond of $[Fe_2(CS)(CO)_3(Cp)_2]$. *Organometallics* **2016**, *35*, 2630−2637. (b) Dyke, A. F.; Knox, S. A. R.; Naish, P. J.; Taylor, G. E. Organic chemistry of dinuclear metal centres. Part 1. Combination of alkynes with carbon monoxide at di-iron and diruthenium centres: crystal structure of $[Ru_2(CO)(\mu\text{-}CO)\{\mu\text{-}\sigma\text{:}\eta^3\text{-}C(O)C_2Ph_2\}(\eta\text{-}C_5H_5)_2]$. *J. Chem. Soc., Dalton Trans.* **1982**, 1297−1307.
(28) As a comparison, the solubility of cisplatin in H_2O is estimated to be 3 $g{\cdot}L^{-1}$.[29]

https://doi.org/10.1021/acs.organomet.1c00519
Organometallics 2022, 41, 514−526

(29) Marloye, M.; Berger, G.; Gelbcke, M.; Dufrasne, F. A. A survey of the mechanisms of action of anticancer transition metal complexes. *Future Med. Chem.* **2016**, *8*, 2263−2286.
(30) (a) Kitzman, H. H.; McMahon, R. J.; Williams, M. G.; Frost, S. C. Effect of Glucose Deprivation on GLUT 1 Expression in 3T3-Ll Adipocytes. *J. Biol. Chem.* **1993**, *268*, 1320−1325. (b) Lodge, J.; Jacobson, G. R. Starvation-Induced Stimulation Of Sugar Uptake In Streptococcus Mutans Is Due To An Effect On The Activities Of Preexisting Proteins Of The Phosphotransferase System. *Infect. Immun.* **1988**, *56*, 2594−2600. (c) Wertheimer, E.; Sassont, S.; Cerasi, E.; Ben-Neriah, Y. The ubiquitous glucose transporter GLUT-1 belongs to the glucose-regulated protein family of stress-inducible proteins. *Proc. Natl. Acad. Sci. U.S.A.* **1991**, *88*, 2525−2529. (d) Koivisto, U.-M.; Martinez-Valdez, H.; Bilan, P. J.; Elena Burdett, E.; Ramlal, T.; Klip, A. Differential Regulation of the GLUT-1 and GLUT-4 Glucose Transport Systems by Glucose and Insulin in L6 Muscle Cells in Culture. *J. Biol. Chem.* **1991**, *266*, 2615−2621.
(31) Liang, C.; Park, A. Y.; Guan, J. In vitro scratch assay: a convenient and inexpensive method for analysis of cell migration in vitro. *Nat. Protoc.* **2007**, *2*, 329−333.
(32) (a) Rocco, D.; Busto, N.; Pérez-Arnaiz, C.; Biancalana, L.; Zacchini, S.; Pampaloni, G.; Garcia, B.; Marchetti, F. Antiproliferative and bactericidal activity of diiron and monoiron cyclopentadienyl carbonyl complexes comprising a vinyl-aminoalkylidene unit. *Appl. Organomet. Chem.* **2020**, *34*, No. e5923. (b) Marzenell, P.; Hagen, H.; Sellner, L.; Zenz, T.; Grinyte, R.; Pavlov, V.; Daum, S.; Mokhir, A. Aminoferrocene-Based Prodrugs and Their Effects on Human Normal and Cancer Cells as Well as Bacterial Cells. *J. Med. Chem.* **2013**, *56*, 6935−6944.
(33) Menges, F. *Spectragryph—Optical Spectroscopy Software*, version 1.2.5; Spectragryph, 2016−2017. http://www.effemm2.de/spectragryph.
(34) Fulmer, G. R.; Miller, A. J. M.; Sherden, N. H.; Gottlieb, H. E.; Nudelman, A.; Stoltz, B. M.; Bercaw, J. E.; Goldberg, K. I. NMR Chemical Shifts of Trace Impurities: Common Laboratory Solvents, Organics, and Gases in Deuterated Solvents Relevant to the Organometallic Chemist. *Organometallics* **2010**, *29*, 2176−2179.
(35) Willker, W.; Leibfritz, D.; Kerssebaum, R.; Bermel, W. Gradient selection in inverse heteronuclear correlation spectroscopy. *Magn. Reson. Chem.* **1993**, *31*, 287−292.
(36) Albano, V. G.; Busetto, L.; Monari, M.; Zanotti, V. Reactions of acetonitrile di-iron μ-aminocarbyne complexes; synthesis and structure of $[Fe_2(\mu\text{-}CNMe_2)(\mu\text{-}H)(CO)_2(Cp)_2]$. *J. Organomet. Chem.* **2000**, *606*, 163−168.
(37) Rundlöf, T.; Mathiasson, M.; Bekiroglu, S.; Hakkarainen, B.; Bowden, T.; Arvidsson, T. Survey and qualification of internal standards for quantification by ^{1}H NMR spectroscopy. *J. Pharm. Biomed. Anal.* **2010**, *52*, 645−651.
(38) Rice, N. M.; Irving, H. M. N. H.; Leonard, M. A. Nomenclature for liquid-liquid distribution (solvent extraction) (IUPAC Recommendations 1993). *Pure Appl. Chem.* **1993**, *65*, 2373−2396.
(39) Biancalana, L.; Batchelor, L. K.; Funaioli, T.; Zacchini, S.; Bortoluzzi, M.; Pampaloni, G.; Dyson, P. J.; Marchetti, F. α-Diimines as Versatile, Derivatizable Ligands in Ruthenium(II) p-Cymene Anticancer Complexes. *Inorg. Chem.* **2018**, *57*, 6669−6685.

https://doi.org/10.1021/acs.organomet.1c00519
Organometallics 2022, 41, 514−526